Title: Intestinal organoids expose heterogeneity in SARS-CoV-2 susceptibility

Kyung Ku Jang[1], Maria E Kaczmarek[2#], Simone Dallari[1], Ying-Han Chen[1], Jordan Axelrad[3], Kenneth A Stapleford[2*] and Ken Cadwell[1,2,3*]

[1] Kimmel Center for Biology and Medicine at the Skirball Institute, New York Grossman University School of Medicine, New York, NY, USA

[2] Department of Microbiology, New York University Grossman School of Medicine, New York, NY 10016, USA.

[3] Division of Gastroenterology and Hepatology, Department of Medicine, New York University Grossman School of Medicine, New York, NY 10016, USA.

#Present address: EcoHealth Alliance in New York, NY 10018

*Correspondence:
Ken Cadwell
Email: ken.cadwell@med.nyu.edu
Kenneth Stapleford
Email: kenneth.stapleford@nyulangone.org

ABSTRACT

Organoids generated from primary human specimens facilitate investigation of the intestinal barrier by recreating the complex cellular composition of the epithelium. Although the significance remains unclear, intestinal organoid lines display heterogeneity in their growth and morphology. We hypothesized that organoids will also display variability in the degree to which they are susceptible to infectious agents. Using SARS-CoV-2 as a model, we found orders of magnitude differences in the amount of SARS-CoV-2 recovered from small intestinal and colonic organoids generated from different donors. SARS-CoV-2 burden did not correlate with demographic or clinical features associated with donors, but rather reflected the expression level of the virus receptor *ACE2*. Remarkably, organoid *ACE2* transcript levels matched the amount of ACE2 detected in primary tissue from the same individual, indicating that certain properties of the intestinal epithelium are retained during *ex vivo* differentiation. Longitudinal transcriptomics of organoids identified a delayed yet robust interferon signature, the magnitude of which corresponded to the degree of SARS-CoV-2 infection. These results suggest that intestinal organoids display substantial heterogeneity in their ability to support viral infections and can potentially inform mechanisms behind interindividual differences in susceptibility to infectious disease.

MAIN TEXT

Intestinal organoid cultures have transformed our ability to investigate properties of the human intestinal epithelium. Consisting of organized epithelial cell clusters differentiated from somatic stem cells, intestinal organoids generated from endoscopic pinch biopsies are capable of self-renewal and recreate many of the structural, functional, and molecular characteristics of the tissue of origin (1). Investigators have exploited these versatile properties of intestinal organoids to study infectious agents that are otherwise difficult to examine, including viruses such as noroviruses (2-4). Intestinal organoids can also inform our understanding of inter-individual differences in disease susceptibility, such as elucidating the mechanisms by which mutations accumulate in patients with colorectal cancer (5, 6). Additionally, we and others have documented substantial heterogeneity in the growth, morphology, viability, and susceptibility to cytokine toxicity of human intestinal organoid lines (1, 6-8). However, how this heterogeneity relates to resistance of the intestinal epithelium to infectious agents remains unclear.

Although severe acute respiratory syndrome coronavirus 2 (SARS-CoV-2) infection is primarily associated with dysfunction of the respiratory system, the gastrointestinal (GI) tract is also an established target organ in patients with COVID-19. As many as 60% of patients present with diarrhea, vomiting, abdominal pain, anorexia, and/or nausea (9-16). Also, SARS-CoV-2 antigen in intestinal biopsies and viral RNA in the stool are readily detected, even after the virus is undetectable in respiratory samples (17-27). To a limited extent, virions and infectious particles have been detected in patient intestinal and stool specimens (17, 25, 28, 29). Although the pathophysiological significance of these observations has not been resolved, the prolonged presence of viral antigens in the gut is likely to impact antibody evolution (17). Consistent with a potential intestinal tropism, intestinal epithelial cells display robust expression of the SARS-CoV-2 receptor angiotensin I converting enzyme 2 (ACE2) and transmembrane proteases TMPRSS2 and TMPRSS4 that facilitate viral entry (30-32). Further, human intestinal organoids derived from either somatic stem cells or inducible pluripotent stem cells (iPSCs) support SARS-CoV-2 reproduction (32-35). These studies have shown that *ACE2* expression levels can differ based on the differentiation state and anatomical region from which the organoids are derived, but whether this affects the degree of SARS-CoV-2 infection is debated. A broader comparison of gene expression patterns and SARS-CoV-2 infection across organoids from different donors and culture conditions may help interpret the studies that have highlighted the extreme range of *ACE2* expression in intestinal tissues associated with demographic and clinical features of individuals, which could have consequences for susceptibility to both viral infections and inflammatory conditions (36-42)

81 To determine the degree to which *ACE2*, *TMPRSS2*, and *TMRPSS4* were differentially
82 expressed between donors and culture conditions, we established and differentiated 3D organoid
83 lines from small intestinal and colonic biopsies procured from 8 and 10 donors, respectively
84 (Supplemental Table 1). Consistent with previous observations (32, 33), the expression of *ACE2*,
85 *TMPRSS2,* and the enterocyte marker of differentiation *APOA1* were significantly higher in small
86 intestinal and colonic organoid lines cultured in 3D differentiation media (3DD) compared with
87 those cultured in expansion media (3DE) that maintains organoids in an undifferentiated state
88 (Supplemental Fig. 1A, B and D). *TMRPSS4* expression was similar in both conditions
89 (Supplemental Fig. 1C). Donor-to-donor variability in expression was apparent for all four genes.
90 Intestinal organoids can be grown as differentiated monolayers to expose the apical side and
91 facilitate viral entry. We found that the level of *ACE2*, *TMPRSS2*, *TMPRSS4*, and *APOA1*
92 expression in monolayer organoids correlated well with 3DD organoids generated from the same
93 donor (Fig. 1A), suggesting that organoid lines retain their intrinsic gene expression patterns
94 independent of these two culturing conditions. In addition, we found that monolayer organoids
95 exhibited the highest *ACE2* and *TMPRSS2* expression among the culture conditions we examined
96 (Fig. 1B and C). Therefore, we used the monolayer model to perform all subsequent analyses.
97 Finally, we investigated whether *ACE2*, *TMPRSS2*, or *TMPRSS4* expression differed between
98 small intestinal and colonic biopsy monolayers. Although *ACE2* expression did not differ between
99 organoids derived from the small intestine versus colon, *TMPRSS*2 and *TMRPSS4* expression
100 were higher and *APOA1* was decreased in colonic organoids (Fig. 1F-I). The lack of correlation
101 between *ACE2* or *TMPRSS2* expression and *APOA1* expression suggested that heterogeneous
102 *ACE2* and *TMPRSS2* levels were not an artifact caused by insufficient differentiation
103 (Supplemental Fig. 2A and B).
104 Given that organoids were derived from healthy donors and patients with inflammatory
105 bowel disease (IBD) of both sexes, we examined whether these donor attributes contribute to
106 differences in gene expression patterns. When we segregated the data based on disease status
107 or sex in either small intestinal or colonic organoids, we did not observe significant differences in
108 *ACE2, TMPRSS2*, *TMPRSS4*, or *APOA1* (Supplemental Fig. 2C-E). The expression of
109 representative interferon stimulated genes (ISGs) *ISG15*, *OASL,* and *MX2* were also not
110 correlated with disease status or sex, although we note that *ISG15* and *OASL* transcripts were
111 higher in colonic versus small intestinal organoids (Supplemental Fig. 3A and B). These
112 transcripts generally did not correlate with the age of subjects (Supplemental Table 2).
113 *ACE2* expression differed by as much as 6.5-fold when comparing organoids with the
114 highest and lowest expression of this gene (Fig. 2A). To test whether such differences lead to

115 heterogeneity in viral infection, we infected organoids with SARS-CoV-2 at a multiplicity of
116 infection (MOI) of 4 for 72 hrs. Remarkably, the amount of virus detected in the supernatant of
117 culture media by plaque assay differed by as much as 423-fold (Fig. 2B-C). Immunofluorescence
118 microscopy analyses of ACE2 and SARS-CoV-2 nucleoprotein (NP) in representative organoids
119 confirmed these findings – SI1 and C1 (susceptible small intestinal and colonic organoids,
120 respectively, with high *ACE2* transcript levels) displayed higher degrees of ACE2 and NP staining
121 compared with SI7 and C8 (resistant small intestinal and colonic organoids, respectively) (Fig. 2D
122 and E). Indeed, SARS-CoV-2 infection correlated with *ACE2* gene expression levels, but not
123 *TMPRSS2*, *TMPRSS4,* and *APOA1* expression (Fig. 2F-I). The amount of virus recovered from
124 organoids were comparable when the data was segregated by the disease status and sex of the
125 donors (Supplemental Fig. 3D). Similarly, virus production did not correlate with donor age
126 (Supplemental Fig. 3E).

127 The association between susceptibility of organoids to SARS-CoV-2 infection and *ACE2*
128 expression was clear in most cases, but there were outliers for the colonic organoids. For instance,
129 C5 and C8 have moderate to high levels of ACE2 but low levels of virus production (Fig. 2A and
130 B). Thus, we investigated whether other factors may contribute to differential SARS-CoV-2
131 infectivity. Several polymorphisms are predicted to alter the stability of ACE2 or alter its affinity to
132 the SARS-CoV-2 S protein (43-46). However, the sequence of the *ACE2* coding region of C5 and
133 C8 were identical to other donors (Supplemental Table 1). Differences in interferon responses
134 may also contribute to SARS-CoV-2 infectivity, where higher ISG levels are predicted to confer
135 protections against viral infection (47-49). Baseline *ISG15*, *OASL*, and *MX2* expression did not
136 correlate with lower virus production. Instead, we noticed a positive correlation between *OASL*
137 and SARS-CoV-2 susceptibility (Supplemental Fig. 3F-H). Next, we examined ISG expression
138 following stimulation with interferon-beta (IFNβ) or interferon-lambda 2 (IFNλ2). Although we
139 observed varied levels of ISG induction, they were not associated with reduced viral infection
140 (Supplemental Fig. 4A; Supplemental Table 3). Generally, we did not detect an association
141 between the degree to which these ISGs were induced and properties of the donor tissue location,
142 disease status, and age (Supplemental Fig. 4A to C and Supplemental Table 3). However, small
143 intestinal organoids from female donors displayed higher ISG expression than male donors
144 following IFNλ2 stimulation (Supplemental Fig. 4D and E). *ACE2* and *TMPRSS2* expression were
145 not altered by IFNβ or IFNλ2 (Supplemental Fig. 5), indicating that *ACE2* and *TMPRSS2* are not
146 ISGs in monolayer organoids.

147 Our results thus far are consistent with the possibility that *ACE2* gene expression is a key
148 determinant of the degree to which the intestinal epithelium of an individual is susceptible to

149 SARS-CoV-2 infection. As organoids are differentiated from primary stem cells and expanded in
150 culture (50, 51), it was unclear whether inter-donor differences reflect ACE2 levels in the primary
151 tissues. Therefore, we measured ACE2 protein by immunofluorescence microscopy in small
152 intestinal and colonic sections from the same donors corresponding to individual lines of
153 organoids (Fig. 3). ACE2 staining was restricted to the epithelium and most intense along the
154 apical brush boarder (villi in the small intestine and top of the crypts in the colon; Fig. 3A and B
155 and Supplemental Fig. 6), consistent with our data and previous studies showing that *ACE2*
156 expression is enriched in differentiated enterocytes (32, 33). Primary tissue specimens also
157 displayed heterogeneous ACE2 protein levels (Fig.3C and Supplemental Fig. 6C). Remarkably,
158 the mean intensity of ACE2 in intestinal tissue sections strongly correlated with *ACE2* transcript
159 and SARS-CoV-2 levels in organoids derived from the same individual, and not with age, sex, or
160 disease status (Fig. 3E). Therefore, organoids retain the variable ACE2 levels from its original
161 tissue.

162 To further investigate how susceptible and resistant organoids differ from each other, we
163 selected the three colonic organoid lines that each displayed high infection (HI; C1, C2, and C7)
164 or low infection (LI; C8, C9, and C10) for RNA-seq analysis. We validated the transcriptional and
165 microscopy analyses (Fig. 2A, C, and D) by Western blot, which showed higher levels of ACE2
166 protein in HI compared with LI organoids, and comparable levels of TMPRSS2 protein (Fig. 4A).
167 We then infected the organoids with SARS-CoV-2 for 24 and 72 hrs (I24 and I72, respectively),
168 and compared these samples with mock infected organoids harvested at 0 and 72 hrs (UI0 and
169 UI72, respectively). Because these six organoid lines were prepared from independently thawed
170 batches of frozen stocks, we quantified virus and confirmed that higher amounts of SARS-CoV-2
171 were recovered from HI compared with LI organoids at both time points (Fig. 4B and C). Similar
172 to our findings with IFN-stimulated organoids (Supplemental Fig. 5), *ACE2* and *TMPRESS2*
173 transcripts in both HI and LI organoids were stable during the course of infection (Supplemental
174 Fig. 7A and B).

175 The number of transcripts displaying >2-fold changes (adjusted *P*-value <0.05) in 12
176 pairwise comparisons are summarized in Supplemental Fig. 7C. The conditions that displayed
177 the most differences from one another were those comparing early time points to 72 hrs post-
178 infection. Uninfected organoids at 0 and 72 hrs displayed no differences, indicating that the
179 transcriptome of uninfected HI and LI organoids remained stable over time. This result increased
180 our confidence that organoids were fully differentiated at the onset of our experiments. Also, few
181 genes displayed differential expression when comparing uninfected HI and LI organoids. Principal
182 component analysis (PCA) showed that infection (at 72 hrs) separated samples on PC1 and

183 susceptibility to infection (HI versus LI) separated samples on PC2 (Supplemental Fig. 7D). PCA
184 also confirmed observations from the pairwise comparison indicating that uninfected organoids
185 and those infected for 24 hrs were transcriptionally similar.

186 At the 72 hr time point, where the largest transcriptional changes occurred between
187 conditions, we found that the majority of the differentially expressed genes (DEGs) when
188 comparing uninfected and infected conditions (55 of 71) were common to LI and HI organoids,
189 while most DEGs (65 of 81) when comparing infected HI and LI organoids were unique to this
190 comparison (Fig. 4D). Gene ontology analyses and Ingenuity Pathway Analysis (IPA) showed
191 that SARS-CoV-2 infection impacts antiviral pathways, especially those related to the interferon
192 response, and that this signature was more pronounced in HI organoids compared with LI
193 organoids following infection (Fig. 4E-G and Supplemental Fig. 7E). Indeed, differentially
194 expressed genes related to the *response to type I IFN* (*SAMHD1*, *NLRC5*, *USP18*, *IFIT1*, *ZBP1*,
195 *SHFL*, *STAT2*, *IRF7*, *SP100*, *MX1*, *OAS3*, *STAT1*, *ISG15*, and *OAS2*) and *JAK-STAT* (*STAT5A*,
196 *STAT1*, *STAT2*, *CCL2*, and *NMI*) included common ISGs, and although these were upregulated
197 in both HI and LI organoids infected by SARS-CoV-2, they were induced to a higher degree in HI
198 organoids (Supplement Fig. 7F and G). Because these ISGs are more highly expressed in HI
199 organoids and not detected at 24 hrs, they are likely a response to the increased degree of
200 infection in these organoids. These results are consistent with other studies suggesting that the
201 interferon response to SARS-CoV-2 is delayed (33, 49, 52, 53). Unexpectedly, multiple genes
202 associated with pathways related to zinc and copper homeostasis were specifically upregulated
203 in LI organoids compared to HI organoids after 72 hrs of infection (Fig 4E, H and Supplemental
204 Fig. 7H). The increased expression of *MT1* genes encoding metallothionines in LI organoids was
205 particularly striking and may be indicative of a stress response activated by viral perturbations in
206 the epithelium (54, 55). Collectively, longitudinal transcriptome analyses identified robust yet late
207 transcriptional changes induced by SARS-CoV-2, the magnitude of which corresponded to the
208 levels of viral infection.

209 When taken together, our results show that human intestinal organoids reveal
210 interindividual differences in responses to viral infection. Organoids showed substantial
211 differences in their susceptibility to SARS-CoV-2 infection, and ACE2 levels were the strongest
212 correlate of susceptibility, agreeing with the finding that the virus preferentially infects mature
213 enterocytes with high *ACE2* expression (32). Although transcriptome analysis identified many
214 differentially expressed genes upon SARS-CoV-2 infection when comparing organoid lines, these
215 differences were not apparent at 24 hrs post-infection, a time point at which the degree of virus
216 infection already diverged between resistant and susceptible organoids. Therefore, these gene

217 expression patterns are unlikely to account for differential susceptibility, and instead, provide a
218 glimpse as to how increased viral replication can affect properties of the intestinal epithelium.
219 Although the presence of SARS-CoV-2 RNA in the gut has been associated with diarrhea in
220 patients with COVID-19 (27), the consequence of intestinal epithelial infection remains largely
221 unclear and an important area of investigation. Extensive experiments in animal models predict
222 that activation of viral RNA sensors trigger immune responses including ISGs that impact the
223 intestinal barrier (56-66).
224 Finally, it is notable that organoids retained the differential ACE2 levels observed in intact
225 primary tissue sections from the same donor. These results indicate that at least some
226 transcriptional properties of the original intestinal epithelium that are individual-specific are
227 retained following *ex vivo* differentiation. If this finding is generalizable, then organoids can be a
228 powerful platform to investigate interindividual differences in infectious disease susceptibility.
229

230 **METHODS**

231 **Human intestinal tissue specimen collection:**

232 Patients with and without IBD were recruited at outpatient colonoscopy performed for colon
233 cancer screening, surveillance, or IBD activity assessment at NYU Langone Health's
234 Ambulatory Care Center, New York, under an NYU Grossman School of Medicine Institutional
235 Review Board–approved study (Mucosal Immune Profiling in Patients with Inflammatory Bowel
236 Disease; S12-01137). Approximately 6 pinch biopsies were obtained from the ascending colon
237 of each patient using a 2.8-mm standard endoscopic biopsy forceps. The inflammation status
238 of tissue was confirmed by endoscopic and histopathological examination. All pinch biopsies
239 were collected in ice-cold complete RPMI (RPMI 1640 medium supplemented with 10% fetal
240 bovine serum (FBS), penicillin/streptomycin/glutamine, and 50 μM 2-mercaptoethanol). Pinch
241 biopsies were then transferred to freezing media (90% FBS + 10% DMSO) in Cryogenic Tubes
242 and stored in liquid nitrogen.

243

244 **Culture of human small intestinal and colonic organoids:**

245 Human organoids were cultured as described previously (7, 58). Pinch biopsies were thawed in
246 PBS and then incubated in Gentle Cell Dissociation Reagent (Stemcell Technologies) on ice for
247 30 min, followed by vigorous pipetting to isolate crypts. The crypts were embedded in 30 μl of
248 Matrigel and cultured with Human IntestiCult™ Organoid Growth Medium (OGM) (Basal Medium
249 and Organoid Supplement, Stemcell Technologies) supplemented with 100 IU Penicillin and 100
250 μg/ml Streptomycin (Corning) and 125 μg/ml Gentamicin (ThermoFisher), herein referred to as
251 expansion medium. The culture medium was changed every 2-3 days. For passaging human
252 organoids, 10 μM Y-27632 were added for the first 2 days. For differentiation, the human
253 organoids were cultured with 1:1 mix of Human IntestiCult™ OGM Basal Medium and DMEM/F-
254 12 (ThermoFisher) in the presence of 100 IU Penicillin and 100 μg/ml Streptomycin, 125 μg/ml
255 Gentamicin and 2 mM L-Glutamine (Corning), herein referred to as differentiation medium. To
256 generate monolayers, mature human small intestinal colonic organoids grown with the expansion
257 media were digested into single cells using TrypLE Express (ThermoFisher) and seeded into
258 Matrigel-coated 96-well culture plate (Corning) in Y-27632-supplemented expansion medium at
259 150,000 cells/well for the first 2 days. The culture media were changed every day. In experiments
260 in which organoids were treated with recombinant interferons, monolayers grown with the
261 differentiation media for 7 days were stimulated with human IFNβ (100 or 300 IU/ml, R&D systems)
262 or IFNλ2 (10 or 30 ng/ml, R&D systems) for 12 h.

263

264 **Transcript analysis:**

265 Total RNA was extracted from human organoids using RNeasy Mini Kit with DNase treatment
266 (QIAGEN), and synthesis of cDNA was conducted with High-Capacity cDNA Reverse
267 Transcription Kit (ThermoFisher) according to the manufacturer's protocol. RT-PCR was
268 performed using SybrGreen (Roche) on a Roch480II Lightcycler using the following primers:
269 *ACE2*, Fwd 5'-TCAAGGAGGCCGAGAAGTTC-3' and Rev 5'-TTCCTGGGTCCGTTAGCATG-3';
270 *TMPRSS2*, Fwd 5'-ACCTGATCACACCAGCCATG-3' and Rev 5'-
271 CTTCGAAGTGACCAGAGGCC-3'; *TMPRSS4*, Fwd 5'-CCGATGTGTTCAACTGGAAG-3' and
272 Rev 5'-GAGAAAGTGAGTGGGAACTG-3'; *APOA1*, Fwd 5'-TGGATGTGCTCAAAGACAGC-3'
273 and Rev 5'-AGGCCCTCTGTCTCCTTTTC-3'; *ISG15*, Fwd 5'-GAGAGGCAGCGAACTCATCT-3'
274 and Rev 5'-CTTCAGCTCTGACACCGACA-3'; *OASL*, Fwd 5'-AAAGAGAGGCCCATCATCC-3'
275 and Rev 5'-ATCTGGGTAACCCCTCTG C-3'; *MX2*, Fwd 5'-CAGCCACCACCAGGAAACA-3' and
276 Rev 5'-TTCTGCTCGTACTGGCTGTACAG-3'; *GAPDH*, Fwd 5'-GATGGGATTTCCATTGAT
277 GACA-3' and Rev 5'-CCACCCATGGCAAATTCC-3'; SARS-CoV-2 NP, Fwd 5'-
278 ATGCTGCAATCGTGCTACAA-3'; SARS-CoV-2 N, Rev 5'- GACTGCCGCCTCTGCTC-3'.
279 Relative expression of the respective genes to *GAPDH* expression was calculated using the $\Delta\Delta C_T$
280 method. Where indicated, the values were expressed as fold change from uninfected or untreated
281 organoids.

282

283 **Virus infection and plaque assay:**

284 The organoid monolayers grown with the differentiation media for 7 days were infected with
285 icSARS-CoV-2-mNG (isolate USA/WA/1/2020) obtained from the UTMB World Reference
286 Center for Emerging Viruses and Arboviruses (67). A working stock of SARS-CoV-2-mNG was
287 generated by infecting a 90-95% confluent monolayer of Vero E6 cells (ATCC CRL-1586) for
288 48 hrs at 37°C. Following incubation, the supernatant was collected, centrifuged at 1,200 rpm
289 for 5 mins, aliquoted and stored at -80°C. Viral titers were quantified by plaque assay as
290 described below. For the infection, organoid monolayers were infected with SARS-CoV-2-mNG
291 at a MOI of 4 for 1 hr at 37°C. Following incubation, organoids were washed 4 times with
292 phosphate buffered saline (PBS) and differentiation media was added for the indicated time.
293 Total virus in the 3rd or 4th wash was also quantified to ensure excess virus was removed. Thus,
294 virus quantified at the end of the experiment can be assessed as replicative particles rather than
295 residual particles persisting in culture. Viral titers in the monolayer supernatants were quantified
296 by plaque assay.

297 To quantify infectious virus by plaque assay, 10-fold serial dilutions of each sample
298 were made in Dulbecco's Modified Eagle Medium (DMEM). Each dilution was added to a
299 monolayer of Vero E6 cells for 1 hr at 37°C. Following incubation, DMEM supplemented with
300 2% fetal bovine serum and 0.8% agarose was added and the incubated for 72 hrs at 37°C. Cells
301 were then fixed with 10% formalin, the agarose plug removed, and wells stained with crystal
302 violet (10% crystal violet, 20% ethanol). Virus titers (PFU/ml) were determined by counting the
303 number of plaques on the lowest countable dilution.
304
305 ***ACE2* sequencing:**
306 A 2418-bp region containing the *ACE2* coding region was amplified from cDNA prepared from
307 organoids (see above) by PCR using a pair of primers (Fwd 5'-ATGTCAAGCTCTTCCTGGCTCC-
308 3' and Rev 5'-CTAAAAGGAGGTCTGAACATCATCAGTG-3'). Amplicons were cloned into
309 pCR™2.1-TOPO® (Invitrogen). The plasmids were sequenced by Sanger sequencing from
310 Psomagen using 4 primers: M13F, 5'-GTAAAACGACGGCCAGT-3'; M13R, 5'-
311 CAGGAAACAGCTATGAC-3'; ACE2_600F, 5'- GGGGATTATTGGAGAGGAGACT-3';
312 ACE2_1800R, 5'- GTCGGTACTCCATCCCACA-3'.
313
314 **Immunofluorescence:**
315 ACE2 staining were performed as described previously (68). Briefly, pinch biopsies of the terminal
316 ileum and ascending colon were fixed in 10% formalin and embedded in paraffin blocks. Sections
317 were cut to 5 µm thickness at the NYU Center for Biospecimen Research and Development and
318 mounted on frosted glass slides. For deparaffinization, slides were baked at 70°C for 1.5 h,
319 followed by rehydration in descending concentration of ethanol (100%, 95%, 80%, 70%, ddH_2O
320 twice; each step for 30 s). HIER was performed in a pressure cooker (Biocare Medical) using
321 Dako Target Retrieval Solution, pH 9 (Dako Agilent) at 97°C from 10 min and cooled down to
322 65°C. After further cooling to room temperature for 20 min, slides were washed for 10 min 3 times
323 in Tris-Buffered Saline (TBS), containing 0.1% Tween 20 (Sigma; TBS-T). Sections were blocked
324 in 5% normal donkey serum (Sigma) in TBS-T at room temperature (RT) for 1 hr, followed by
325 incubation with rabbit anti-ACE2 antibody (1:100, Abcam, ab15348) in the blocking solution at
326 4°C overnight. Sections were washed 3 times with TBS-T and stained with the Alexa Flour 555
327 conjugated with donkey anti-rabbit IgG (1:500, ThermoFisher, A-31572) in PBS with 3% bovine
328 serum albumin (BSA) (ThermoFisher), 0.4% saponin, and 0.02% sodium azide at RT for 1 hr.
329 Following this, sections were washed 3 times with TBS-T and mounted with ProLong™ Glass
330 Antifade Mountant with NucBlue™ Stain (ThermoFisher, P36918). Images were acquired using

331 an EVOS FL Auto Cell Imaging System (ThermoFisher) and then processed and quantified using
332 ImageJ.
333 SARS-CoV-2-infected monolayers were fixed with 4% paraformaldehyde (Electron
334 Microscopy Sciences) for 3 hrs at RT. Following fixation, cells were washed 3 times with PBS
335 then blocked and permeabilized in PBS with 0.1% Triton-X100 and 3% BSA for 0.5 hr at RT. The
336 permeabilized organoids were washed 3 times with PBS and incubated with mouse anti-SARS-
337 CoV-2 N antibody (1:1,000, ProSci, 10-605) and rabbit anti-ACE2 antibody (1:500, Abcam,
338 ab15348) diluted in PBS containing 3% BSA overnight at 4°C. The monolayers were washed 3
339 times with PBS and stained with Alexa Flour 647 conjugated with goat anti mouse IgG (1:2,000,
340 ThermoFisher, A32728) and Alexa Flour 594 conjugated with donkey anti rabbit IgG (1:1,000,
341 ThermoFisher, 21207) diluted in PBS with 3% BSA and 4'6-diamidino-2-phenylindole (DAPI) for
342 1 hr at RT. The monolayers were then washed 3 times with PBS and imaged using the CellInsight
343 CX7 High-content Microscope (ThermoFisher).
344
345 **Immunoblotting:**
346 Organoids were processed for immunoblotting as previously described (66). Briefly, monolayers
347 were incubated in lysis buffer (20 mM Tris-HCl (pH 7.4), 150 mM NaCl, 1% Triton X-100, 10%
348 glycerol, and 2x Halt Protease and Phosphatase Inhibitor Cocktail (ThermoFisher) on ice for 5
349 min and centrifuged at 14,000 rpm for 20 min. Samples were resolved on Bolt 4-12% Bis-Tris
350 Plus Gels (Invitrogen), transferred onto PVDF membranes, and blocked using 5% skim milk.
351 The following antibodies were used for immunoblotting studies: mouse anti-β-actin (1:5,000,
352 Sigma, AC-15), rabbit anti-ACE2 (1:1,000, Abcam, ab15348), mouse anti-TMPRSS2 (1:1,000,
353 Santa Cruz, sc-515727). Secondary antibodies (mouse anti-rabbit and goat-anti mouse, 211-
354 032-171 and 115-035-174, respectively) were purchased from JacksonImmunoResearch
355
356 **RNA deep sequencing and analysis:**
357 Organoid monolayers were cultured in differentiation media for 7 days and then were infected
358 with SARS-CoV-2 at MOI of 4 for 24 hrs or 72 hrs before RNA extraction with 2-3 technical
359 duplicates per line. CEL-seq2 was performed on 53 human organoids RNA samples.
360 Sequencing was performed on Illumina NovaSeq 6000 (Illumina). RNA-seq results were
361 processed using the R package "DESeq2" to obtain variance stabilized count reads, fold
362 changes relative to specific condition, and statistical *P*-value. Analysis of the organoid

363 transcriptome focused on differentially expressed genes, defined as the genes with an absolute
364 fold change relative to specific condition >2 and an adjusted *P*-value <0.05.
365

366 **Computational and statistical analysis**

367 Gene ontology analysis was performed using the R package "clusterProfiler". Principal
368 Component Analysis was performed using the R package "stats". Heatmaps were generated
369 using the R package "pheatmap". Upstream regulators analysis was performed by uploading
370 the differentially expressed genes to Ingenuity Pathway Analysis software (Qiagen).

371 Statistical differences were determined as described in figure legend using either R or
372 GraphPad Prism 9 software (La Jolla, CA, USA).
373

374 **Data availability**

375 The accession number for the gene expression raw data reported in this paper is GSE179949.
376
377

FUNDING

This research was supported by NIH grants DK093668 (K.C.), AI121244 (K.C.), HL123340 (K.C.), AI130945 (K.C.), AI140754 (K.C.), DK124336 (K.C.), and a pilot award from the NYU CTSA grant UL1TR001445 from the National Center for Advancing Translational Sciences (NCATS) (K.C.). Additional support was provided by the Faculty Scholar grant from the Howard Hughes Medical Institute (K.C.), Crohn's & Colitis Foundation (K.C.), Kenneth Rainin Foundation (K.C.), Judith & Stewart Colton Center of Autoimmunity (K.C.). K.C. is a Burroughs Wellcome Fund Investigator in the Pathogenesis of Infectious Diseases. M.E.K was supported by a Public Health Service Institutional Research Training Award T32 AI7647.

DECLARATION OF INTERESTS

K.C. has received research support from Pfizer, Takeda, Pacific Biosciences, Genentech, and Abbvie. K.C. has consulted for or received an honoraria from Puretech Health, Genentech, and Abbvie. K.C. holds U.S. patent 10,722,600 and provisional patent 62/935,035 and 63/157,225.

ACKNOWLEDGMENTS

We wish to thank the NYU Grossman School of Medicine Center for Biospecimen Research and Development, Microscopy Lab, and Flow Cytometry and Cell Sorting, Microscopy, Genome Technology, and Histology Cores (supported by National Institutes of Health [NIH] grants P31CA016087, S10OD01058, and S10OD018338) for technical assistance and Dr. Meike Dittmann at the NYU Grossman School of Medicine for use of the CX7 CellInsight high-content microscope.

AUTHOR CONTRIBUTION

Conceptualization: Kyung Ku Jang, Kenneth Stapleford, Ken Cadwell
Data curation: Kyung Ku Jang, Kenneth Stapleford, Ken Cadwell
Formal analysis: Kyung Ku Jang, Maria E Kaczmarek, Ying-Han Chen, Simone Dallari
Funding acquisition: Kenneth Stapleford, Ken Cadwell
Investigation: Kyung Ku Jang, Maria E Kaczmarek, Ying-Han Chen, Simone Dallari, Kenneth Stapleford
Methodology: Kyung Ku Jang, Maria E Kaczmarek, Ying-Han Chen, Simone Dallari, Kenneth Stapleford
Project administration: Kenneth Stapleford, Ken Cadwell
Resources: Kyung Ku Jang, Maria E Kaczmarek, Ying-Han Chen, Simone Dallari, Jordan Axelrad
Supervision: Kenneth Stapleford, Ken Cadwell
Validation: Kyung Ku Jang, Maria E Kaczmarek, Ying-Han Chen, Simone Dallari
Visualization: Kyung Ku Jang, Maria E Kaczmarek, Simone Dallari
Writing – original draft: Kyung Ku Jang, Simone Dallari, Jordan Axelrad, Kenneth Stapleford, Ken Cadwell
Writing – review & editing: Kyung Ku Jang, Maria E Kaczmarek, Ying-Han Chen, Simone Dallari, Jordan Axelrad, Kenneth Stapleford, Ken Cadwell

422 **Figure 1. Heterogeneous expression of *ACE2*, *TMPRSS2*, and *TMPRSS4* in small intestinal**
423 **and colonic organoids.**
424 **(A)** Correlation analysis of *ACE2* and *TMPRSS2* (left) or *TMPRSS4* and *APOA1* (right) expression
425 in human intestinal (circle) and colonic (rectangle) organoids cultured as monolayers grown in
426 differentiation media for 7 days with those cultured as human 3D organoids grown in
427 differentiation media (3DD) for 7 days. **(B-E)** RT-PCR data comparing *ACE2* (B), *TMPRSS2* (C),
428 *TMPRSS4* (D), *APOA1* (E), expression in human 3D organoids grown with expansion media
429 (3DE), 3DD, and monolayers grown in differentiation media for 7 days. **(F-I)** RT-PCR analysis of
430 *ACE2* (F), *TMPRSS2* (G), *TMPRSS4* (H), and *APOA1* (I) expression among human small
431 intestine (SI)- or colon-derived monolayers grown in differentiation media for 7 days. Data points
432 are mean of 3 technical replicates of individual organoid lines. Bars represent mean ± SEM, and
433 at least 2 independent experiments were performed. r, Pearson correlation coefficient. *$P \leq 0.05$,
434 **$P \leq 0.01$, ***$P \leq 0.001$, and ****$P \leq 0.0001$ by simple regression analysis in A, paired *t* test, two
435 tailed in B-E, and unpaired *t* test, two-tailed in F-I.
436
437 **Figure 2. Differential susceptibility of intestinal organoids correlates with *ACE2* expression.**
438 **(A)** RT-PCR analysis of *ACE2* expression in small intestinal (SI1-SI8) and colonic (C1-C10)
439 organoid monolayers. **(B)** Plaque forming units (PFU) determined by virus titration on Vero E6
440 cells of supernatant from monolayers at 72 hrs post-infection with SARS-CoV-2. **(C)** PFU of
441 SARS-CoV-2 according to tissue location. **(D)** Representative immunofluorsence microscopy
442 images showing co-staining of DAPI (blue), ACE2 (green), and SARS-CoV-2 nucleoprotein (NP)
443 (red) in SARS-CoV-2 infected SI1, SI7, C1, and C8 organoid lines. An image of uninfected C1 is
444 shown as a representative uninfected condition and a Matrigel-coated well without organoids is
445 shown as a control for background fluorescence. **(E)** Total intensity of NP and ACE2 normalized
446 with cell counts of SI1, SI7, C1 and C8. **(F-I)** Correlation of SARS-CoV2 PFU with *ACE2* (F),
447 *TMPRSS2* (G), *TMPRSS4* (H), or *APOA1* (I) expression among organoid monolayers. Data points
448 in A, B, and E are each technical replicate, and data points in C and F-I are the mean of 3 technical
449 replicates of individual organoid lines. Bars represent mean ± SEM, and at least 2 independent
450 experiments were performed. SI, small intestine; r, Pearson correlation coefficient. *$P \leq 0.05$ and
451 ***$P \leq 0.001$ by simple regression analysis in F-I.
452
453 **Figure 3. Differential *ACE2* expression observed in individual intestinal organoid lines are**
454 **conserved in primary tissue from the same donor.**

455 **(A and B)** Representative ACE2 staining images in primary tissues of terminal ileum (A) and
456 ascending colon (B) from which SI1, SI7, C1, and C10 organoids were established. **(C)** Mean
457 intensity of ACE2 per area (right) in each field of view from the primary tissues from which small
458 intestinal and colonic organoids were established. **(D)** Mean intensity of ACE2 by disease (left) or
459 sex (right). **(E)** Correlation of ACE2 mean intensity with *ACE2* expressions (left) and SARS-CoV-
460 2 PFU (middle) among organoids or subject age (right). Data points in C are the field of views,
461 and data points in D and E are mean of 3 technical replicates of individual organoid lines. Bars
462 represent mean ± SEM, and at least 2 independent experiments were performed. Bars: 200 μm.
463 SI, small intestine; r, Pearson correlation coefficient. *$P \leq 0.05$, **$P \leq 0.01$, and ***$P \leq 0.001$ by
464 unpaired *t* test, two-tailed in D and simple regression analysis in E.
465
466 **Figure 4. Transcriptome analysis reveals a heighted and delayed interferon response to**
467 **SARS-CoV-2 infection in susceptible organoids.**
468 **(A)** Western blot analysis of ACE2, TMPRSS2, and ACTB in high infection (HI; C1, C2, and C7)
469 and low infection (LI; C8, C9, and C10) lines. Blots are representative of at least 3 independent
470 repeats. **(B)** PFU determined by virus titration on Vero E6 cells of supernatant of HI and LI at 24
471 and 72 hrs after infection with SARS-CoV-2. **(C)** RT-PCR analysis of SARS-CoV-2 expression in
472 HI and LI organoids upon 24 and 72 hrs infection with SARS-CoV-2. **(D)** Venn diagram depicting
473 the number and overlap of differentially expressed genes (DEGs) according to RNA-Seq analysis
474 (see Supplemental Fig. 7) of HI or LI organoids infected with SARS-CoV-2 for 72 hrs. **(E)** Highly
475 enriched biological process GO terms for the DEGs in HI and LI infected with SARS-CoV-2. **(F**
476 **and G)** Ingenuity pathway analysis (IPA) of the transcriptome of SARS-CoV-2-infected HI or LI
477 for upstream regulators. Interferon-related genes (F) or Top 5 molecules within the classes
478 *cytokine, transcription regulator, transmembrane receptor, ligand-dependent nuclear receptor,*
479 *and others* (G) commonly associated with HI infected/uninfected and LI infected/uninfected
480 conditions. **(H)** DEGs of LI infected/HI infected condition were analyzed by IPA for upstream
481 regulators. Top 5 upstream regulators related to Zn ion homeostasis and interferons for the LI.
482 Data points in B and C represent the mean of technical replicates of individual organoids lines.
483 Bars represent mean ± SEM, and at least 2 independent experiments were performed. *$P \leq 0.05$,
484 and **$P \leq 0.01$, by unpaired *t* test, two-tailed in B and C.
485
486 **Supplemental figure 1. Transcriptional analysis of *ACE2*, *TMPRSS2*, *TMPRSS4*, and *APOA1***
487 **in 3D intestinal organoids cultured in different media conditions.**

488 **(A-D)** RT-PCR analysis of *ACE2 (A)*, *TMPRSS2* (B), and *TMPRSS4* (C), and *APOA1* (D)
489 expression among small intestinal (SI) or colonic (C) 3D organoids grown in expansion media
490 (3DE) or differentiation media (3DD) for 7 days. Data points are mean of 3 technical replicates of
491 individual organoid lines. Bars represent mean, and at least 2 independent experiments were
492 performed. $^{**}P \leq 0.01$, $^{***}P \leq 0.001$, and $^{****}P \leq 0.0001$ by paired *t* test, two-tailed.
493
494 **Supplemental figure 2. Transcript analysis of organoid monolayers according to tissue**
495 **location, disease, and sex of subjects.**
496 **(A and B)** Correlation of *ACE2* (A) and *TMPRSS2* (B) expression with *APOA1* expression among
497 organoid monolayers grown in differentiation media for 7 days. **(C)** RT-PCR analysis of *ACE2*
498 expression among organoid monolayers grown in differentiation media according to the disease
499 status or sex of subjects. **(D and E)** RT-PCR data depicting *ACE2*, *TMPRSS2*, *TMPRSS4*,
500 *APOA1*, *ISG15*, *OASL*, and *MX2* expression of organoid monolayers grown in differentiation
501 media for 7 days according to disease (D) or sex (E). Data points are mean of 3 technical
502 replicates of individual organoid lines. Bars represent mean ± SEM, and at least 2 independent
503 experiments were performed. SI, small intestine; r, Pearson correlation coefficient. The indicated
504 *P*-values by unpaired *t* test, two-tailed in C.
505
506 **Supplemental figure 3. Analysis of gene expression and viral replication in organoids by**
507 **intestinal region, disease, sex, or age of subjects.**
508 **(A-C)** RT-PCR analysis of *ISG15* (A), *OASL* (B), and *MX2* (C) expression in organoid monolayers.
509 **(D)** PFU of SARS-CoV-2 according to disease status or sex (right) of subjects. **(E-H)** Correlation
510 of PFU of SARS-CoV-2 with age of subjects (E) or *ISG15* (F), *OASL* (G), and *MX2* (H) expression.
511 Data points are mean of 3 technical replicates of individual organoid lines. Bars represent mean
512 ± SEM, and at least 2 independent experiments were performed. SI, small intestine; r, Pearson
513 correlation coefficient. $^{*}P \leq 0.05$ and $^{***}P \leq 0.001$ by unpaired *t* test, two-tailed in A-D and simple
514 regression analysis in E-H.
515
516 **Supplemental figure 4. Transcript analysis of IFNβ- or IFNλ2-stimulated organoids**
517 **according to intestinal region, disease status, or sex of subjects.**
518 **(A-E)** RT-PCR data depicting fold change in *ISG15*, *OASL*, and *MX2* expression in small intestinal
519 and colonic organoid monolayers stimulated with IFNβ (100 or 300 IU/ml) or IFNλ2 (10 or 30
520 ng/ml) for 12 hrs according to intestinal region (A), disease status (B and C) or sex (D and E) of
521 subjects. Each value is normalized to non-stimulated organoid lines. Data points are mean of 3

522 technical replicates of individual organoid lines. Bars represent mean ± SEM, and at least 2
523 independent experiments were performed. SI, small intestine. *$P \leq 0.05$ and **$P \leq 0.01$ by
524 unpaired *t* test, two-tailed.
525
526 **Supplemental figure 5. Stimulation with IFNβ or IFNλ2 does not alter *ACE2* and *TMPRSS2***
527 **expression in organoids.**
528 **(A and B)** RT-PCR depicting *ACE2* (A) and *TMPRSS2* (B) expression in organoid monolayers
529 stimulated with IFNβ (100 or 300 IU/ml) or IFNλ2 (10 or 30 ng/ml) for 12 hrs. Data points are mean
530 of 3 technical replicates of individual organoid lines. Bars represent mean ± SEM, and at least 2
531 independent experiments were performed. SI, small intestine.
532
533 **Supplemental figure 6. Representative images of ACE2 staining in primary intestinal tissue.**
534 **(A and B)** Representative ACE2 staining images in primary tissues of terminal ileum from which
535 small intestinal (SI2-SI6 and S8, A) or colonic (C2-C9, B) monolayers were established. Images
536 of remaining organoids are included in main Figure 3. **(C)** Quantification of the total intensity of
537 ACE2 staining and surface area in each visual field from the primary tissues from which the
538 indicated organoid lines were established. Data points in C are the visual field. Bars in A and B:
539 200 μm. Bars in C represent mean ± SEM.
540
541 **Supplemental figure 7. Transcriptome of SARS-CoV-2-infected organoids.**
542 **(A and B)** RT-PCR data depicting *ACE2* (A) and *TMPRSS2* (B) expression in high infection (HI;
543 C1, C2, and C7) and low infection (LI; C8, C9, and C10) lines with or without SARS-CoV-2
544 infection. **(C)** Number of up- and down-regulated genes identified by RNA-Seq analysis in the
545 indicated pair-wise comparison of HI and LI organoids lines at different time point post infection.
546 n = 3 organoid lines per group and at least 2 technical replicates per individual organoid line. **(D)**
547 Unsupervised clustering based on expression of most variable genes by organoids lines and
548 infection with SARS-CoV-2 at 24 and 72 hrs. **(E)** Highly enriched molecular function GO terms for
549 the differentially expressed genes (DEGs) in HI and LI infected with SARS-CoV-2 for 72 hrs. **(F**
550 **and G)** Heatmaps displaying normalized expression values of DEGs in HI infected/uninfected and
551 LI infected/uninfected conditions (average fold-change ≥ 2 and adjusted *P*-value ≤ 0.05)
552 annotated in GO:0060338 and GO:0034340 (F) and GO0:07259 (G) **(H)** Heatmap displaying
553 normalized expression values of DEGs in LI infected/HI infected conditions (average fold-change
554 ≥ 2 and adjusted *P*-value ≤ 0.05) annotated in GO:0006882. Data points are mean of at least 2

555 technical replicates of individual organoid lines. Bars represent mean ± SEM. UI0, uninfected 0
556 hr; UI72, uninfected 72 hrs; I24, infected for 24 hrs, I72, infected for 72 hrs.
557

558 **Table S1**

Name	Tissue	Sex	Age	Disease type	Inflammation	*ACE2* SNP
SI1	Terminal ileum	F	47	Non-IBD	Non-inflamed	ND
SI2	Terminal ileum	M	23	CD	Non-inflamed	ND
SI3	Terminal ileum	M	37	CD	Non-inflamed	NA
SI4	Terminal ileum	F	25	Non-IBD	Non-inflamed	NA
SI5	Terminal ileum	M	29	Non-IBD	Non-inflamed	ND
SI6	Terminal ileum	M	47	CD	Non-inflamed	ND
SI7	Terminal ileum	F	67	CD	Non-inflamed	ND
SI8	Terminal ileum	M	37	CD	Non-inflamed	NA
C1	Ascending colon	M	34	Non-IBD	Non-inflamed	ND
C2	Ascending colon	M	25	Non-IBD	Non-inflamed	NA
C3	Ascending colon	F	27	UC	Non-inflamed	NA
C4	Ascending colon	M	33	UC	Non-inflamed	NA
C5	Ascending colon	M	33	UC	Non-inflamed	ND
C6	Ascending colon	M	29	Non-IBD	Non-inflamed	ND
C7	Ascending colon	F	55	UC	Non-inflamed	NA
C8	Ascending colon	F	23	Non-IBD	Non-inflamed	ND
C9	Ascending colon	M	21	UC	Non-inflamed	NA
C10	Ascending colon	F	20	UC	Non-inflamed	ND

559

560 **Supplemental Table 1**. Subject information for human endoscopic specimens

561 M; Male, F; Female, CD; Crohn's disease; UC; Ulcerative colitis; SNP, Single nucleotide

562 polymorphism; ND, not detected; NA, not attempted

563

564

565

566 **Table S2**

Gene expression	Age					
	SI + Colon		SI		Colon	
	r	*P*	r	*P*	r	*P*
ACE2	-0.100	0.694	-0.509	0.197	0.456	0.186
TMPRSS2	-0.208	0.408	-0.186	0.659	0.066	0.857
TMPRSS4	0.203	0.420	0.195	0.644	0.023	0.950
APOA1	0.318	0.199	0.10	0.813	-0.285	0.425
ISG15	-0.297	0.232	-0.287	0.490	-0.118	0.745
OASL	0.113	0.656	0.018	0.967	0.690	0.027*
MX2	0.033	0.896	0.064	0.881	-0.148	0.684

567

568 **Supplemental Table 2**. Correlation between subject age and gene expression among the
569 organoid monolayers grown in differentiation media for 7 days. *r*, Pearson correlation coefficient;
570 *P*, *P*-value; SI, small intestine. *$P \leq 0.05$ by simple regression analysis

571

572 **Table S3**

Gene induction	Age				SARS-CoV-2 replication			
	SI		Colon		SI		Colon	
	r	*P*	*r*	*P*	*r*	*P*	*r*	*P*
ISG15								
100 IU/ml IFNβ	0.190	0.652	-0.202	0.576	0.213	0.612	0.104	0.775
300 IU/ml IFNβ	0.239	0.569	-0.118	0.745	0.146	0.731	-0.149	0.682
10 ng/ml IFNλ2	0.208	0.622	-0.271	0.449	0.012	0.977	-0.305	0.391
30 ng/ml IFNλ2	0.295	0.478	-0.167	0.645	-0.261	0.533	-0.118	0.745
OASL								
100 IU/ml IFNβ	0.884	0.004**	-0.293	0.412	-0.436	0.281	-0.227	0.529
300 IU/ml IFNβ	0.796	0.018*	0.196	0.412	-0.173	0.682	-0.143	0.694
10 ng/ml IFNλ2	0.458	0.254	-0.078	0.830	-0.412	0.31	-0.486	0.154
30 ng/ml IFNλ2	0.554	0.155	0.616	0.058	-0.341	0.409	-0.360	0.307
MX2								
100 IU/ml IFNβ	-0.211	0.616	-0.104	0.775	0.483	0.226	-0.078	0.831
300 IU/ml IFNβ	0.032	0.941	-0.050	0.892	0.499	0.208	-0.196	0.587
10 ng/ml IFNλ2	-0.464	0.247	-0.147	0.687	0.032	0.939	-0.337	0.342
30 ng/ml IFNλ2	0.247	0.556	0.075	0.837	0.019	0.965	-0.129	0.722

573

574 **Supplemental Table 3**. Correlation of subject age or PFU of SARS-CoV-2 with ISG induction in
575 organoids stimulated with IFNβ (100 or 300 IU/ml) or IFNλ2 (10 or 30 ng/ml) for 12 hrs. *r*, Pearson
576 correlation coefficient; *P*, *P*-value; SI, small intestine. *$P \leq 0.05$ and **$P \leq 0.01$ by simple
577 regression analysis.

578

579

580

581 **References**

582 1. Fujii M, Sato T. Somatic cell-derived organoids as prototypes of human epithelial tissues
583 and diseases. Nat Mater. 2020.
584 2. Geiser P, Di Martino ML, Samperio Ventayol P, Eriksson J, Sima E, Al-Saffar AK, et al.
585 Salmonella enterica Serovar Typhimurium Exploits Cycling through Epithelial Cells To
586 Colonize Human and Murine Enteroids. mBio. 2021;12(1).
587 3. Finkbeiner SR, Zeng XL, Utama B, Atmar RL, Shroyer NF, Estes MK. Stem cell-
588 derived human intestinal organoids as an infection model for rotaviruses. mBio.
589 2012;3(4):e00159-12.
590 4. Hosmillo M, Chaudhry Y, Nayak K, Sorgeloos F, Koo BK, Merenda A, et al. Norovirus
591 Replication in Human Intestinal Epithelial Cells Is Restricted by the Interferon-Induced
592 JAK/STAT Signaling Pathway and RNA Polymerase II-Mediated Transcriptional Responses.
593 mBio. 2020;11(2).
594 5. Drost J, Clevers H. Organoids in cancer research. Nat Rev Cancer. 2018;18(7):407-18.
595 6. Nanki K, Fujii M, Shimokawa M, Matano M, Nishikori S, Date S, et al. Somatic
596 inflammatory gene mutations in human ulcerative colitis epithelium. Nature.
597 2020;577(7789):254-9.
598 7. Matsuzawa-Ishimoto Y, Hine A, Shono Y, Rudensky E, Lazrak A, Yeung F, et al. An
599 intestinal organoid-based platform that recreates susceptibility to T-cell-mediated tissue injury.
600 Blood. 2020;135(26):2388-401.
601 8. Borten MA, Bajikar SS, Sasaki N, Clevers H, Janes KA. Automated brightfield
602 morphometry of 3D organoid populations by OrganoSeg. Sci Rep. 2018;8(1):5319.
603 9. Luo X, Zhou GZ, Zhang Y, Peng LH, Zou LP, Yang YS. Coronaviruses and
604 gastrointestinal diseases. Mil Med Res. 2020;7(1):49.
605 10. Ye L, Yang Z, Liu J, Liao L, Wang F. Digestive system manifestations and clinical
606 significance of coronavirus disease 2019: A systematic literature review. J Gastroenterol
607 Hepatol. 2020.
608 11. D'Amico F, Baumgart DC, Danese S, Peyrin-Biroulet L. Diarrhea During COVID-19
609 Infection: Pathogenesis, Epidemiology, Prevention, and Management. Clin Gastroenterol
610 Hepatol. 2020;18(8):1663-72.
611 12. Gupta A, Madhavan MV, Sehgal K, Nair N, Mahajan S, Sehrawat TS, et al.
612 Extrapulmonary manifestations of COVID-19. Nat Med. 2020;26(7):1017-32.
613 13. Redd WD, Zhou JC, Hathorn KE, McCarty TR, Bazarbashi AN, Thompson CC, et al.
614 Prevalence and Characteristics of Gastrointestinal Symptoms in Patients With Severe Acute
615 Respiratory Syndrome Coronavirus 2 Infection in the United States: A Multicenter Cohort Study.
616 Gastroenterology. 2020;159(2):765-7 e2.
617 14. Cheung KS, Hung IFN, Chan PPY, Lung KC, Tso E, Liu R, et al. Gastrointestinal
618 Manifestations of SARS-CoV-2 Infection and Virus Load in Fecal Samples From a Hong Kong
619 Cohort: Systematic Review and Meta-analysis. Gastroenterology. 2020;159(1):81-95.
620 15. Nobel YR, Phipps M, Zucker J, Lebwohl B, Wang TC, Sobieszczyk ME, et al.
621 Gastrointestinal Symptoms and Coronavirus Disease 2019: A Case-Control Study From the
622 United States. Gastroenterology. 2020;159(1):373-5 e2.
623 16. Aghemo A, Piovani D, Parigi TL, Brunetta E, Pugliese N, Vespa E, et al. COVID-19
624 Digestive System Involvement and Clinical Outcomes in a Large Academic Hospital in Milan,
625 Italy. Clin Gastroenterol Hepatol. 2020;18(10):2366-8 e3.

626 17. Gaebler C, Wang Z, Lorenzi JCC, Muecksch F, Finkin S, Tokuyama M, et al. Evolution
627 of antibody immunity to SARS-CoV-2. Nature. 2021;591(7851):639-44.
628 18. Morone G, Palomba A, Iosa M, Caporaso T, De Angelis D, Venturiero V, et al.
629 Incidence and Persistence of Viral Shedding in COVID-19 Post-acute Patients With Negativized
630 Pharyngeal Swab: A Systematic Review. Front Med (Lausanne). 2020;7:562.
631 19. Park SK, Lee CW, Park DI, Woo HY, Cheong HS, Shin HC, et al. Detection of SARS-
632 CoV-2 in Fecal Samples From Patients With Asymptomatic and Mild COVID-19 in Korea. Clin
633 Gastroenterol Hepatol. 2020.
634 20. Wolfel R, Corman VM, Guggemos W, Seilmaier M, Zange S, Muller MA, et al.
635 Virological assessment of hospitalized patients with COVID-2019. Nature. 2020;581(7809):465-
636 9.
637 21. Holshue ML, DeBolt C, Lindquist S, Lofy KH, Wiesman J, Bruce H, et al. First Case of
638 2019 Novel Coronavirus in the United States. N Engl J Med. 2020;382(10):929-36.
639 22. Guan WJ, Ni ZY, Hu Y, Liang WH, Ou CQ, He JX, et al. Clinical Characteristics of
640 Coronavirus Disease 2019 in China. N Engl J Med. 2020;382(18):1708-20.
641 23. Xiao F, Tang M, Zheng X, Liu Y, Li X, Shan H. Evidence for Gastrointestinal Infection
642 of SARS-CoV-2. Gastroenterology. 2020;158(6):1831-3 e3.
643 24. Coryell MP, Iakiviak M, Pereira N, Murugkar PP, Rippe J, Williams DB, et al. A
644 method for detection of SARS-CoV-2 RNA in healthy human stool: a validation study. Lancet
645 Microbe. 2021.
646 25. Livanos AE, Jha D, Cossarini F, Gonzalez-Reiche AS, Tokuyama M, Aydillo T, et al.
647 Gastrointestinal involvement attenuates COVID-19 severity and mortality. medRxiv. 2020.
648 26. Effenberger M, Grabherr F, Mayr L, Schwaerzler J, Nairz M, Seifert M, et al. Faecal
649 calprotectin indicates intestinal inflammation in COVID-19. Gut. 2020;69(8):1543-4.
650 27. Britton GJ, Chen-Liaw A, Cossarini F, Livanos AE, Spindler MP, Plitt T, et al. SARS-
651 CoV-2-specific IgA and limited inflammatory cytokines are present in the stool of select patients
652 with acute COVID-19. medRxiv. 2020.
653 28. Xiao F, Sun J, Xu Y, Li F, Huang X, Li H, et al. Infectious SARS-CoV-2 in Feces of
654 Patient with Severe COVID-19. Emerg Infect Dis. 2020;26(8):1920-2.
655 29. Bradley BT, Maioli H, Johnston R, Chaudhry I, Fink SL, Xu H, et al. Histopathology
656 and ultrastructural findings of fatal COVID-19 infections in Washington State: a case series.
657 Lancet. 2020;396(10247):320-32.
658 30. Ziegler CGK, Allon SJ, Nyquist SK, Mbano IM, Miao VN, Tzouanas CN, et al. SARS-
659 CoV-2 Receptor ACE2 Is an Interferon-Stimulated Gene in Human Airway Epithelial Cells and
660 Is Detected in Specific Cell Subsets across Tissues. Cell. 2020;181(5):1016-35 e19.
661 31. Muus C, Luecken MD, Eraslan G, Sikkema L, Waghray A, Heimberg G, et al. Single-
662 cell meta-analysis of SARS-CoV-2 entry genes across tissues and demographics. Nat Med.
663 2021;27(3):546-59.
664 32. Zang R, Gomez Castro MF, McCune BT, Zeng Q, Rothlauf PW, Sonnek NM, et al.
665 TMPRSS2 and TMPRSS4 promote SARS-CoV-2 infection of human small intestinal
666 enterocytes. Sci Immunol. 2020;5(47).
667 33. Lamers MM, Beumer J, van der Vaart J, Knoops K, Puschhof J, Breugem TI, et al.
668 SARS-CoV-2 productively infects human gut enterocytes. Science. 2020;369(6499):50-4.
669 34. Zhou J, Li C, Liu X, Chiu MC, Zhao X, Wang D, et al. Infection of bat and human
670 intestinal organoids by SARS-CoV-2. Nat Med. 2020;26(7):1077-83.

671 35. Stanifer ML, Kee C, Cortese M, Zumaran CM, Triana S, Mukenhirn M, et al. Critical
672 Role of Type III Interferon in Controlling SARS-CoV-2 Infection in Human Intestinal Epithelial
673 Cells. Cell Rep. 2020;32(1):107863.
674 36. Vuille-Dit-Bille RN, Liechty KW, Verrey F, Guglielmetti LC. SARS-CoV-2 receptor
675 ACE2 gene expression in small intestine correlates with age. Amino Acids. 2020;52(6-7):1063-
676 5.
677 37. Penninger JM, Grant MB, Sung JJY. The Role of Angiotensin Converting Enzyme 2 in
678 Modulating Gut Microbiota, Intestinal Inflammation, and Coronavirus Infection.
679 Gastroenterology. 2021;160(1):39-46.
680 38. Potdar AA, Dube S, Naito T, Li K, Botwin G, Haritunians T, et al. Altered Intestinal
681 ACE2 Levels Are Associated With Inflammation, Severe Disease, and Response to Anti-
682 Cytokine Therapy in Inflammatory Bowel Disease. Gastroenterology. 2021;160(3):809-22 e7.
683 39. Suarez-Farinas M, Tokuyama M, Wei G, Huang R, Livanos A, Jha D, et al. Intestinal
684 Inflammation Modulates the Expression of ACE2 and TMPRSS2 and Potentially Overlaps With
685 the Pathogenesis of SARS-CoV-2-related Disease. Gastroenterology. 2021;160(1):287-301 e20.
686 40. Triana S, Metz-Zumaran C, Ramirez C, Kee C, Doldan P, Shahraz M, et al. Single-cell
687 analyses reveal SARS-CoV-2 interference with intrinsic immune response in the human gut. Mol
688 Syst Biol. 2021;17(4):e10232.
689 41. Zhang H, Li HB, Lyu JR, Lei XM, Li W, Wu G, et al. Specific ACE2 expression in
690 small intestinal enterocytes may cause gastrointestinal symptoms and injury after 2019-nCoV
691 infection. Int J Infect Dis. 2020;96:19-24.
692 42. Potdar AA, Dube S, Naito T, Botwin G, Haritunians T, Li D, et al. Reduced expression
693 of COVID-19 host receptor, ACE2 is associated with small bowel inflammation, more severe
694 disease, and response to anti-TNF therapy in Crohn's disease. medRxiv. 2020.
695 43. Lanjanian H, Moazzam-Jazi M, Hedayati M, Akbarzadeh M, Guity K, Sedaghati-Khayat
696 B, et al. SARS-CoV-2 infection susceptibility influenced by ACE2 genetic polymorphisms:
697 insights from Tehran Cardio-Metabolic Genetic Study. Sci Rep. 2021;11(1):1529.
698 44. Guo X, Chen Z, Xia Y, Lin W, Li H. Investigation of the genetic variation in ACE2 on
699 the structural recognition by the novel coronavirus (SARS-CoV-2). J Transl Med.
700 2020;18(1):321.
701 45. Calcagnile M, Forgez P, Iannelli A, Bucci C, Alifano M, Alifano P. Molecular docking
702 simulation reveals ACE2 polymorphisms that may increase the affinity of ACE2 with the SARS-
703 CoV-2 Spike protein. Biochimie. 2021;180:143-8.
704 46. Khayat AS, de Assumpcao PP, Meireles Khayat BC, Thomaz Araujo TM, Batista-
705 Gomes JA, Imbiriba LC, et al. ACE2 polymorphisms as potential players in COVID-19
706 outcome. PLoS One. 2020;15(12):e0243887.
707 47. Busnadiego I, Fernbach S, Pohl MO, Karakus U, Huber M, Trkola A, et al. Antiviral
708 Activity of Type I, II, and III Interferons Counterbalances ACE2 Inducibility and Restricts
709 SARS-CoV-2. mBio. 2020;11(5).
710 48. Cheemarla NR, Watkins TA, Mihaylova VT, Wang B, Zhao D, Wang G, et al.
711 Magnitude and timing of the antiviral response determine SARS-CoV-2 replication early in
712 infection. medRxiv. 2021.
713 49. Lowery SA, Sariol A, Perlman S. Innate immune and inflammatory responses to SARS-
714 CoV-2: Implications for COVID-19. Cell Host Microbe. 2021.

715 50. Sato T, Stange DE, Ferrante M, Vries RG, Van Es JH, Van den Brink S, et al. Long-term
716 expansion of epithelial organoids from human colon, adenoma, adenocarcinoma, and Barrett's
717 epithelium. Gastroenterology. 2011;141(5):1762-72.
718 51. Middendorp S, Schneeberger K, Wiegerinck CL, Mokry M, Akkerman RD, van
719 Wijngaarden S, et al. Adult stem cells in the small intestine are intrinsically programmed with
720 their location-specific function. Stem Cells. 2014;32(5):1083-91.
721 52. Lei X, Dong X, Ma R, Wang W, Xiao X, Tian Z, et al. Activation and evasion of type I
722 interferon responses by SARS-CoV-2. Nat Commun. 2020;11(1):3810.
723 53. Chen X, Saccon E, Appelberg KS, Mikaeloff F, Rodriguez JE, Vinhas BS, et al. Type-I
724 interferon signatures in SARS-CoV-2 infected Huh7 cells. Cell Death Discov. 2021;7(1):114.
725 54. Ghoshal K, Majumder S, Zhu Q, Hunzeker J, Datta J, Shah M, et al. Influenza virus
726 infection induces metallothionein gene expression in the mouse liver and lung by overlapping
727 but distinct molecular mechanisms. Mol Cell Biol. 2001;21(24):8301-17.
728 55. Ilback NG, Glynn AW, Wikberg L, Netzel E, Lindh U. Metallothionein is induced and
729 trace element balance changed in target organs of a common viral infection. Toxicology.
730 2004;199(2-3):241-50.
731 56. Abt MC, Buffie CG, Susac B, Becattini S, Carter RA, Leiner I, et al. TLR-7 activation
732 enhances IL-22-mediated colonization resistance against vancomycin-resistant enterococcus. Sci
733 Transl Med. 2016;8(327):327ra25.
734 57. Kernbauer E, Ding Y, Cadwell K. An enteric virus can replace the beneficial function of
735 commensal bacteria. Nature. 2014;516(7529):94-8.
736 58. Neil JA, Matsuzawa-Ishimoto Y, Kernbauer-Holzl E, Schuster SL, Sota S, Venzon M, et
737 al. IFN-I and IL-22 mediate protective effects of intestinal viral infection. Nat Microbiol.
738 2019;4(10):1737-49.
739 59. Van Winkle JA, Constant DA, Li L, Nice TJ. Selective Interferon Responses of
740 Intestinal Epithelial Cells Minimize Tumor Necrosis Factor Alpha Cytotoxicity. J Virol.
741 2020;94(21).
742 60. Sun L, Miyoshi H, Origanti S, Nice TJ, Barger AC, Manieri NA, et al. Type I
743 Interferons Link Viral Infection to Enhanced Epithelial Turnover and Repair. Cell Host Microbe.
744 2014.
745 61. Aden K, Tran F, Ito G, Sheibani-Tezerji R, Lipinski S, Kuiper JW, et al. ATG16L1
746 orchestrates interleukin-22 signaling in the intestinal epithelium via cGAS-STING. J Exp Med.
747 2018;215(11):2868-86.
748 62. Liu L, Gong T, Tao W, Lin B, Li C, Zheng X, et al. Commensal viruses maintain
749 intestinal intraepithelial lymphocytes via noncanonical RIG-I signaling. Nat Immunol.
750 2019;20(12):1681-91.
751 63. Broggi A, Tan Y, Granucci F, Zanoni I. IFN-lambda suppresses intestinal inflammation
752 by non-translational regulation of neutrophil function. Nat Immunol. 2017;18(10):1084-93.
753 64. Yang JY, Kim MS, Kim E, Cheon JH, Lee YS, Kim Y, et al. Enteric Viruses Ameliorate
754 Gut Inflammation via Toll-like Receptor 3 and Toll-like Receptor 7-Mediated Interferon-beta
755 Production. Immunity. 2016;44(4):889-900.
756 65. Martin PK, Marchiando A, Xu R, Rudensky E, Yeung F, Schuster SL, et al. Autophagy
757 proteins suppress protective type I interferon signalling in response to the murine gut microbiota.
758 Nat Microbiol. 2018;3(10):1131-41.

759 66. Matsuzawa-Ishimoto Y, Shono Y, Gomez LE, Hubbard-Lucey VM, Cammer M, Neil J,
760 et al. Autophagy protein ATG16L1 prevents necroptosis in the intestinal epithelium. J Exp Med.
761 2017;214(12):3687-705.
762 67. Xie X, Muruato A, Lokugamage KG, Narayanan K, Zhang X, Zou J, et al. An Infectious
763 cDNA Clone of SARS-CoV-2. Cell Host Microbe. 2020;27(5):841-8 e3.
764 68. Lee IT, Nakayama T, Wu CT, Goltsev Y, Jiang S, Gall PA, et al. ACE2 localizes to the
765 respiratory cilia and is not increased by ACE inhibitors or ARBs. Nat Commun.
766 2020;11(1):5453.
767

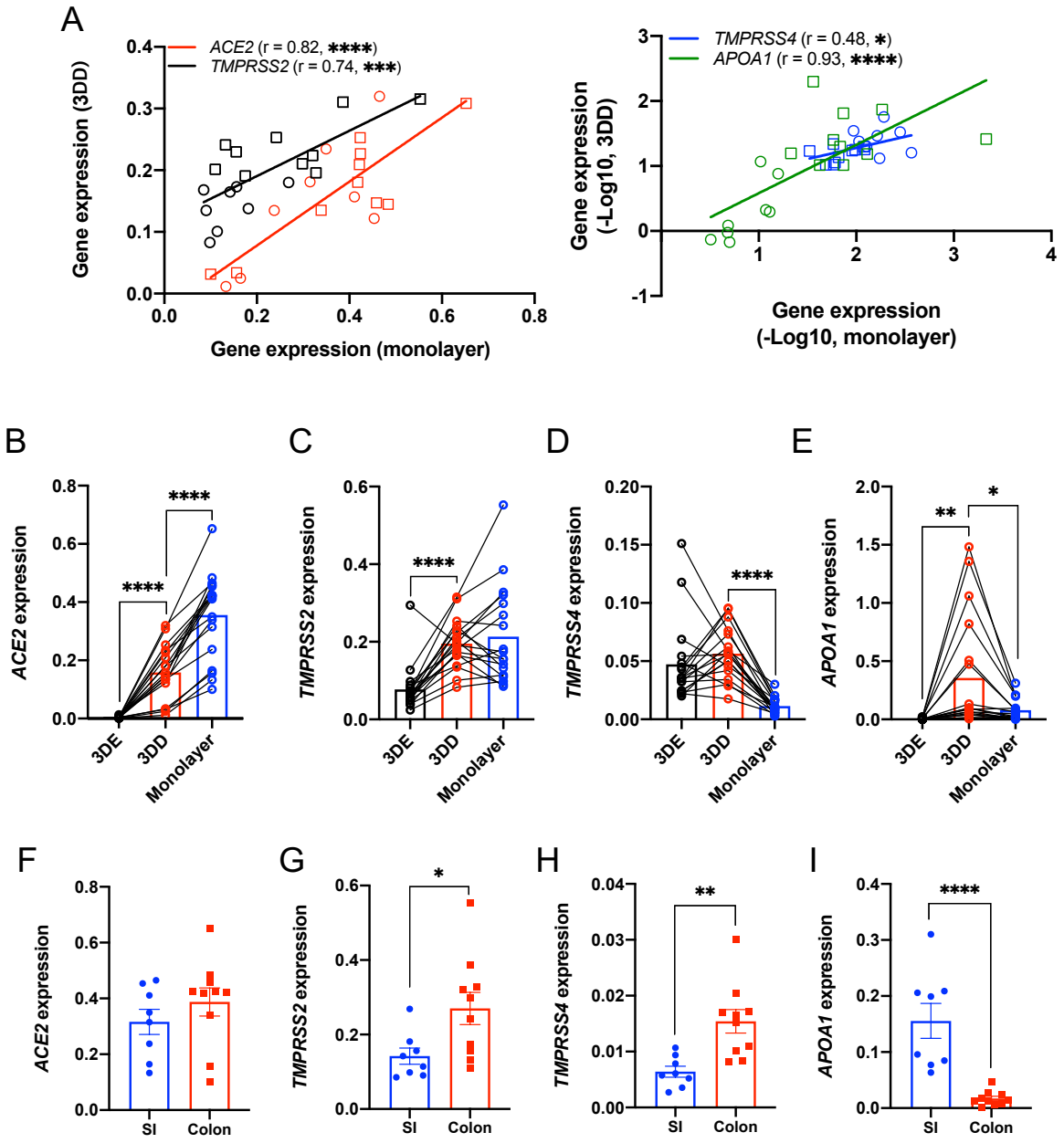
A
ACE2 (r = 0.82, ****)
TMPRSS2 (r = 0.74, ***)
Gene expression (3DD)
Gene expression (monolayer)
TMPRSS4 (r = 0.48, *)
APOA1 (r = 0.93, ****)
Gene expression (-Log10, 3DD)
Gene expression (-Log10, monolayer)
B
ACE2 expression
C
TMPRSS2 expression
D
TMPRSS4 expression
E
APOA1 expression
3DE
3DD
Monolayer
F
ACE2 expression
G
TMPRSS2 expression
H
TMPRSS4 expression
I
APOA1 expression
SI
Colon

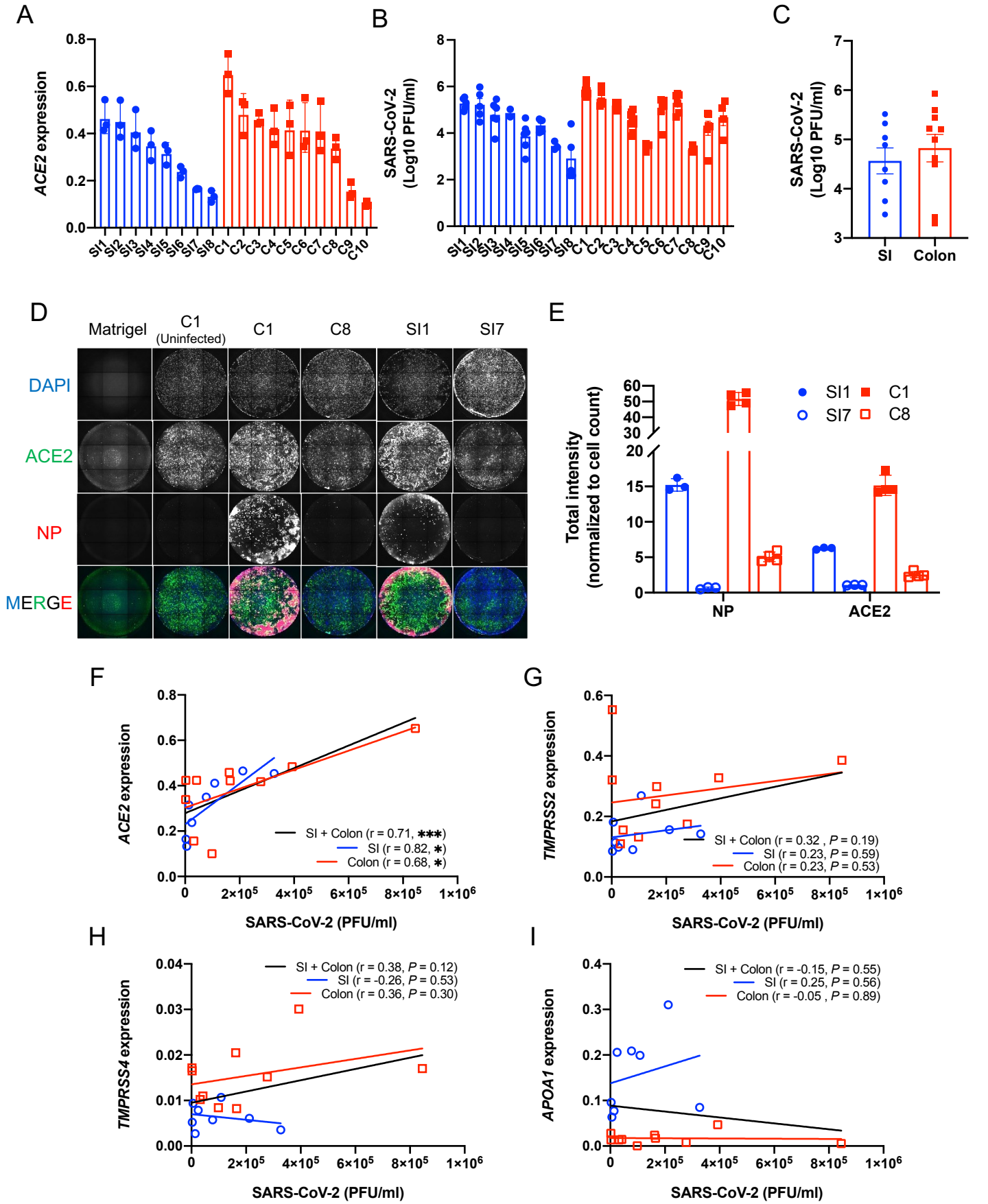
A
ACE2 expression
0.0
0.2
0.4
0.6
0.8
SI1 SI2 SI3 SI4 SI5 SI6 SI7 SI8 C1 C2 C3 C4 C5 C6 C7 C8 C9 C10
B
SARS-CoV-2 (Log10 PFU/ml)
0
2
4
6
8
SI1 SI2 SI3 SI4 SI5 SI6 SI7 SI8 C1 C2 C3 C4 C5 C6 C7 C8 C9 C10
C
SARS-CoV-2 (Log10 PFU/ml)
3
4
5
6
7
SI
Colon
D
Matrigel
C1 (Uninfected)
C1
C8
SI1
SI7
DAPI
ACE2
NP
MERGE
E
Total intensity (normalized to cell count)
0
5
10
15
20
30
40
50
60
SI1
SI7
C1
C8
NP
ACE2
F
ACE2 expression
0.0
0.2
0.4
0.6
0.8
0
2×10^5
4×10^5
6×10^5
8×10^5
1×10^6
SI + Colon (r = 0.71, ***)
SI (r = 0.82, *)
Colon (r = 0.68, *)
SARS-CoV-2 (PFU/ml)
G
TMPRSS2 expression
0.0
0.2
0.4
0.6
0
2×10^5
4×10^5
6×10^5
8×10^5
1×10^6
SI + Colon (r = 0.32 , P = 0.19)
SI (r = 0.23, P = 0.59)
Colon (r = 0.23, P = 0.53)
SARS-CoV-2 (PFU/ml)
H
TMPRSS4 expression
0.00
0.01
0.02
0.03
0.04
0
2×10^5
4×10^5
6×10^5
8×10^5
1×10^6
SI + Colon (r = 0.38, P = 0.12)
SI (r = -0.26, P = 0.53)
Colon (r = 0.36, P = 0.30)
SARS-CoV-2 (PFU/ml)
I
APOA1 expression
0.0
0.1
0.2
0.3
0.4
0
2×10^5
4×10^5
6×10^5
8×10^5
1×10^6
SI + Colon (r = -0.15, P = 0.55)
SI (r = 0.25, P = 0.56)
Colon (r = -0.05 , P = 0.89)
SARS-CoV-2 (PFU/ml)

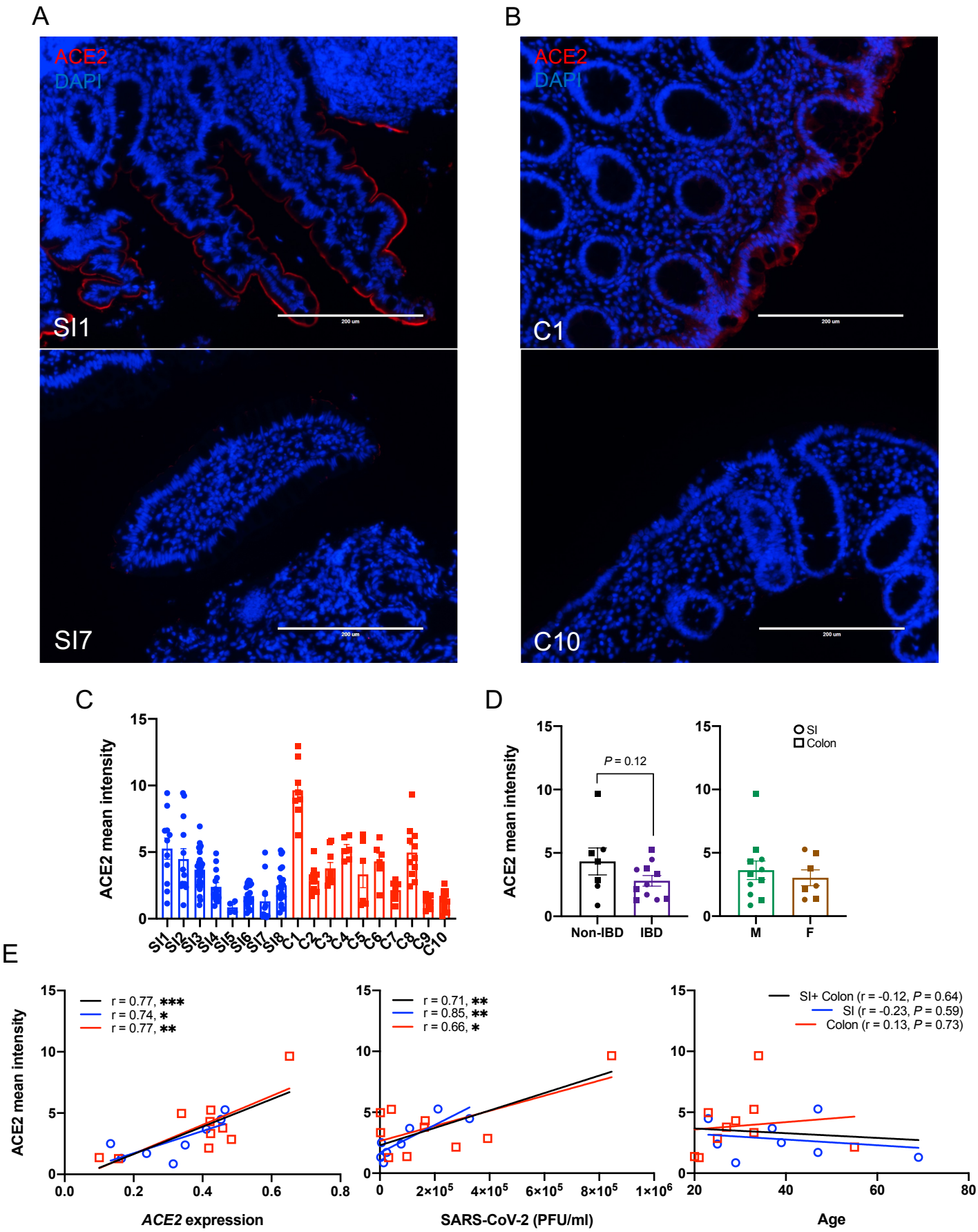
A
ACE2
DAPI
SI1
200 um
SI7
200 um
B
ACE2
DAPI
C1
200 um
C10
200 um
C
ACE2 mean intensity
15
10
5
0
SI1 SI2 SI3 SI4 SI5 SI6 SI7 SI8 C1 C2 C3 C4 C5 C6 C7 C8 C9 C10
D
ACE2 mean intensity
P = 0.12
Non-IBD
IBD
SI
Colon
M
F
E
ACE2 mean intensity
r = 0.77, ***
r = 0.74, *
r = 0.77, **
ACE2 expression
r = 0.71, **
r = 0.85, **
r = 0.66, *
SARS-CoV-2 (PFU/ml)
SI+ Colon (r = -0.12, P = 0.64)
SI (r = -0.23, P = 0.59)
Colon (r = 0.13, P = 0.73)
Age

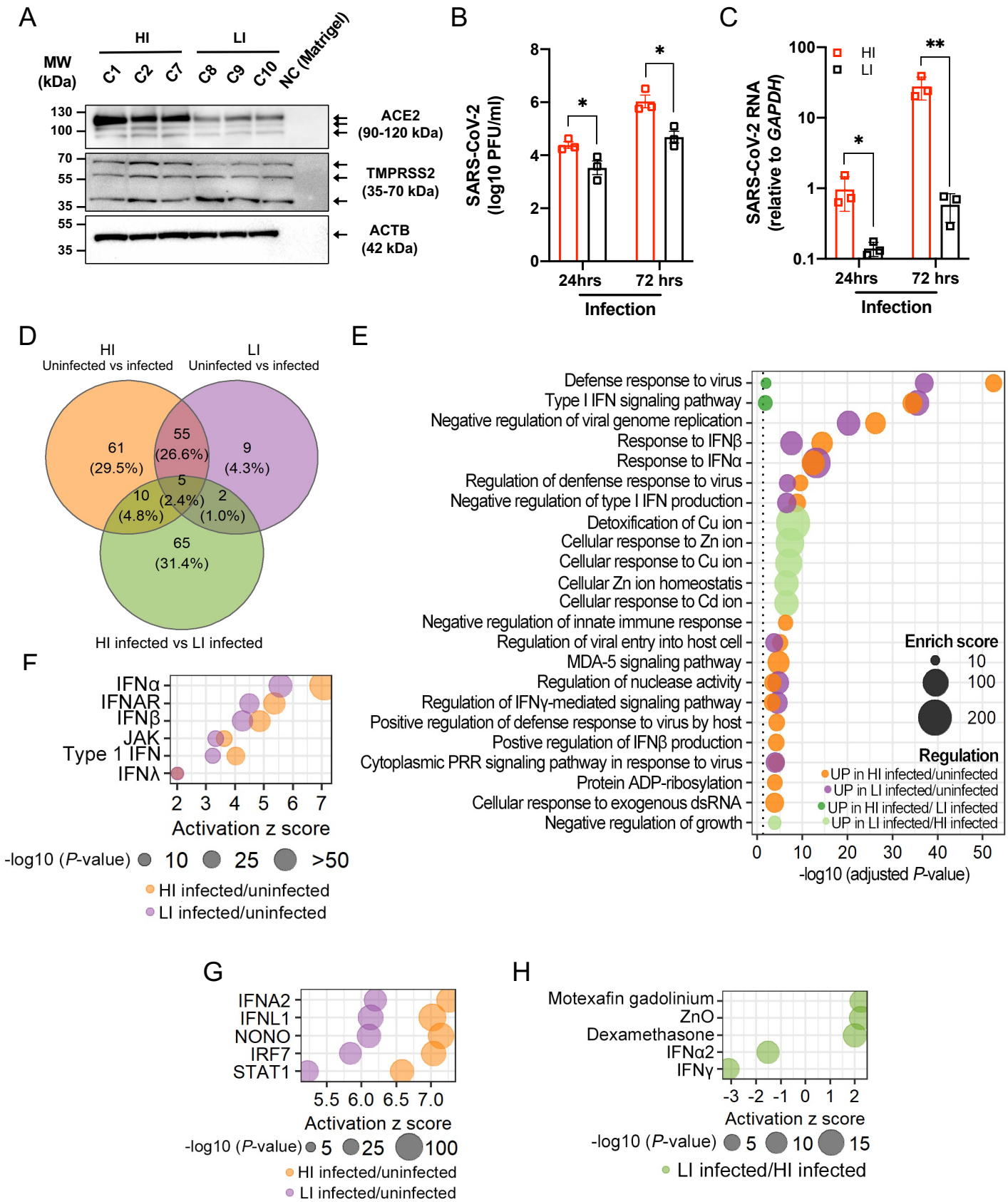
A
HI
LI
MW (kDa)
C1
C2
C7
C8
C9
C10
NC (Matrigel)
130
100
70
55
35
55
35
ACE2 (90-120 kDa)
TMPRSS2 (35-70 kDa)
ACTB (42 kDa)
B
SARS-CoV-2 (log10 PFU/ml)
24hrs
72 hrs
Infection
C
SARS-CoV-2 RNA (relative to GAPDH)
HI
LI
24hrs
72 hrs
Infection
D
HI Uninfected vs infected
LI Uninfected vs infected
61 (29.5%)
55 (26.6%)
9 (4.3%)
5 (2.4%)
10 (4.8%)
2 (1.0%)
65 (31.4%)
HI infected vs LI infected
E
Defense response to virus
Type I IFN signaling pathway
Negative regulation of viral genome replication
Response to IFNβ
Response to IFNα
Regulation of denfense response to virus
Negative regulation of type I IFN production
Detoxification of Cu ion
Cellular response to Zn ion
Cellular response to Cu ion
Cellular Zn ion homeostatis
Cellular response to Cd ion
Negative regulation of innate immune response
Regulation of viral entry into host cell
MDA-5 signaling pathway
Regulation of nuclease activity
Regulation of IFNγ-mediated signaling pathway
Positive regulation of defense response to virus by host
Postive regulation of IFNβ production
Cytoplasmic PRR signaling pathway in response to virus
Protein ADP-ribosylation
Cellular response to exogenous dsRNA
Negative regulation of growth
Enrich score
10
100
200
Regulation
UP in HI infected/uninfected
UP in LI infected/uninfected
UP in HI infected/ LI infected
UP in LI infected/HI infected
-log10 (adjusted P-value)
F
IFNα
IFNAR
IFNβ
JAK
Type 1 IFN
IFNλ
Activation z score
-log10 (P-value) 10 25 >50
HI infected/uninfected
LI infected/uninfected
G
IFNA2
IFNL1
NONO
IRF7
STAT1
Activation z score
-log10 (P-value) 5 25 100
HI infected/uninfected
LI infected/uninfected
H
Motexafin gadolinium
ZnO
Dexamethasone
IFNα2
IFNγ
Activation z score
-log10 (P-value) 5 10 15
LI infected/HI infected

Supplemental Figure 1

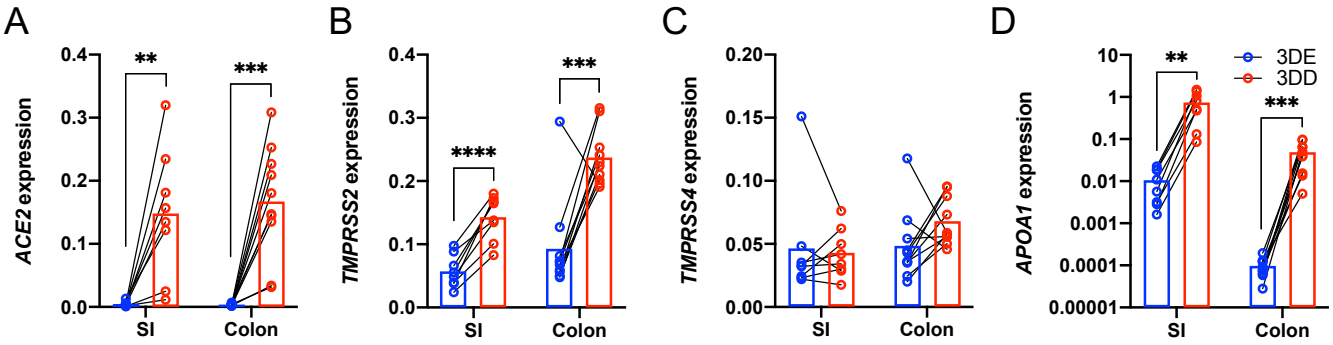

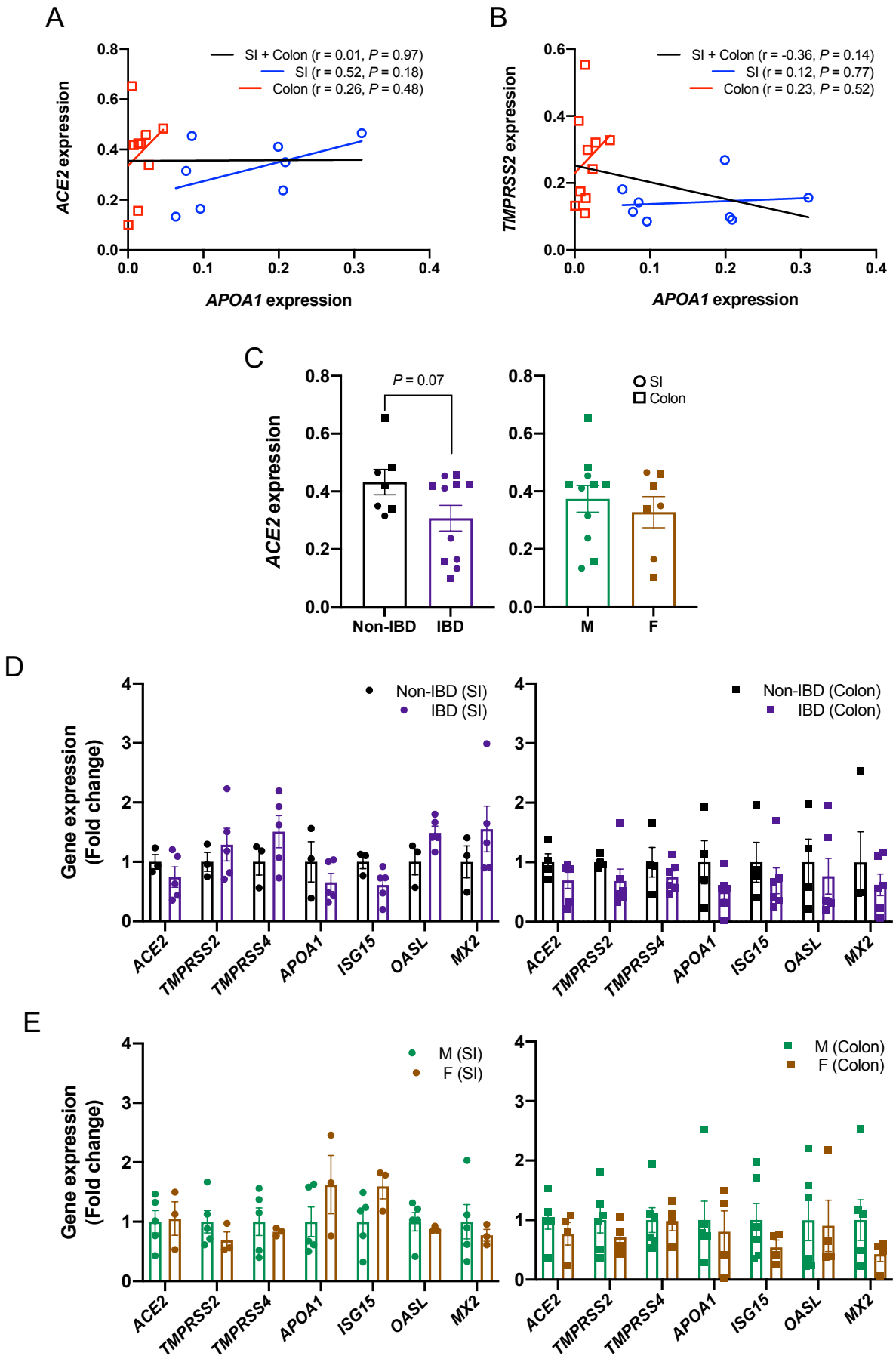
A
SI + Colon (r = 0.01, P = 0.97)
SI (r = 0.52, P = 0.18)
Colon (r = 0.26, P = 0.48)
ACE2 expression
APOA1 expression
B
SI + Colon (r = -0.36, P = 0.14)
SI (r = 0.12, P = 0.77)
Colon (r = 0.23, P = 0.52)
TMPRSS2 expression
APOA1 expression
C
P = 0.07
SI
Colon
ACE2 expression
Non-IBD
IBD
M
F
D
Non-IBD (SI)
IBD (SI)
Non-IBD (Colon)
IBD (Colon)
Gene expression (Fold change)
ACE2
TMPRSS2
TMPRSS4
APOA1
ISG15
OASL
MX2
E
M (SI)
F (SI)
M (Colon)
F (Colon)
Gene expression (Fold change)
ACE2
TMPRSS2
TMPRSS4
APOA1
ISG15
OASL
MX2

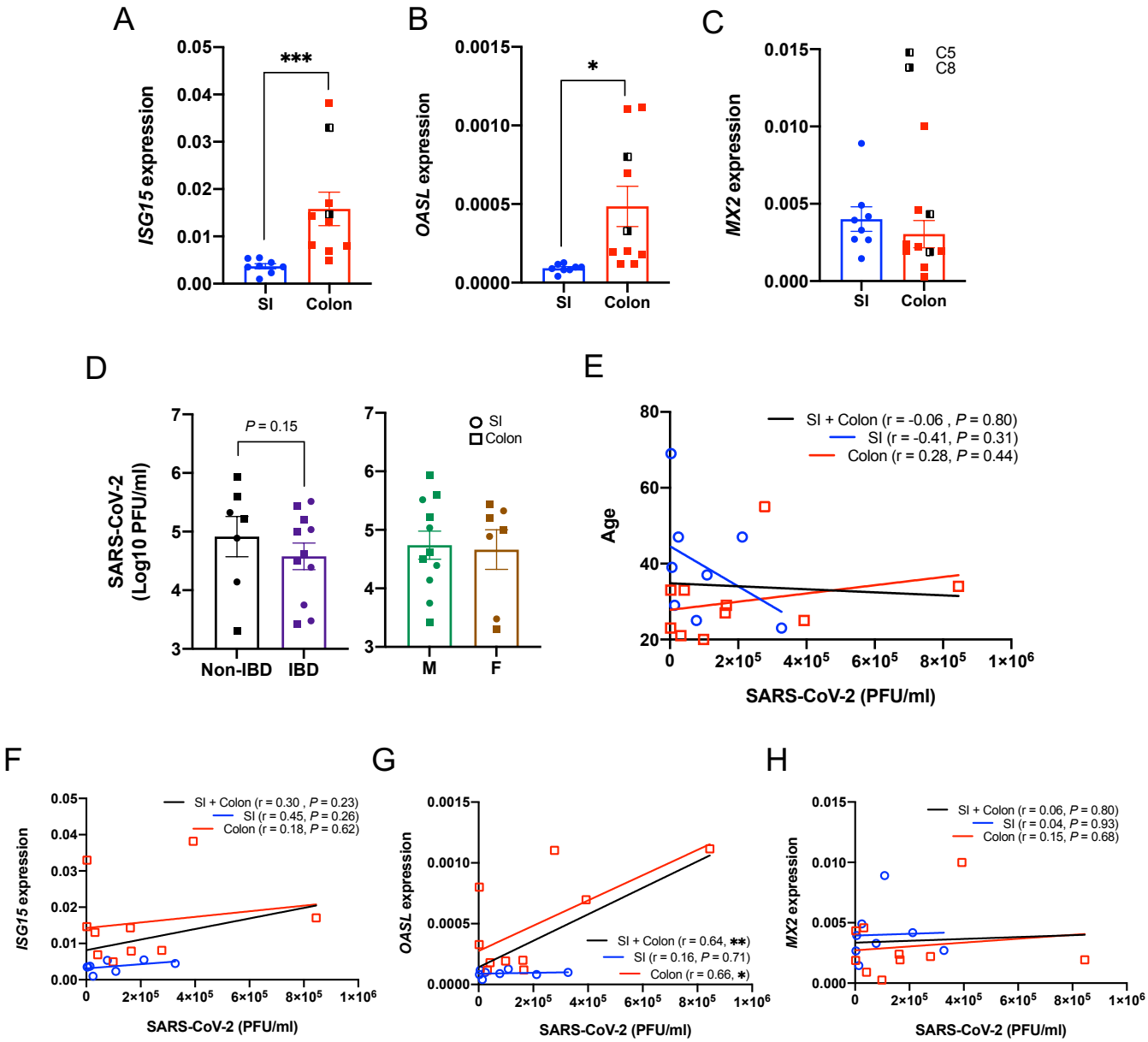
A
ISG15 expression
0.05
0.04
0.03
0.02
0.01
0.00
***
SI
Colon
B
OASL expression
0.0015
0.0010
0.0005
0.0000
*
SI
Colon
C
MX2 expression
0.015
0.010
0.005
0.000
C5
C8
SI
Colon
D
SARS-CoV-2 (Log10 PFU/ml)
7
6
5
4
3
P = 0.15
Non-IBD
IBD
SI
Colon
M
F
E
Age
80
60
40
20
SI + Colon (r = -0.06 , P = 0.80)
SI (r = -0.41, P = 0.31)
Colon (r = 0.28, P = 0.44)
0
2×10^5
4×10^5
6×10^5
8×10^5
1×10^6
SARS-CoV-2 (PFU/ml)
F
ISG15 expression
0.05
0.04
0.03
0.02
0.01
0.00
SI + Colon (r = 0.30 , P = 0.23)
SI (r = 0.45, P = 0.26)
Colon (r = 0.18, P = 0.62)
0
2×10^5
4×10^5
6×10^5
8×10^5
1×10^6
SARS-CoV-2 (PFU/ml)
G
OASL expression
0.0015
0.0010
0.0005
0.0000
SI + Colon (r = 0.64, **)
SI (r = 0.16, P = 0.71)
Colon (r = 0.66, *)
0
2×10^5
4×10^5
6×10^5
8×10^5
1×10^6
SARS-CoV-2 (PFU/ml)
H
MX2 expression
0.015
0.010
0.005
0.000
SI + Colon (r = 0.06, P = 0.80)
SI (r = 0.04, P = 0.93)
Colon (r = 0.15, P = 0.68)
0
2×10^5
4×10^5
6×10^5
8×10^5
1×10^6
SARS-CoV-2 (PFU/ml)

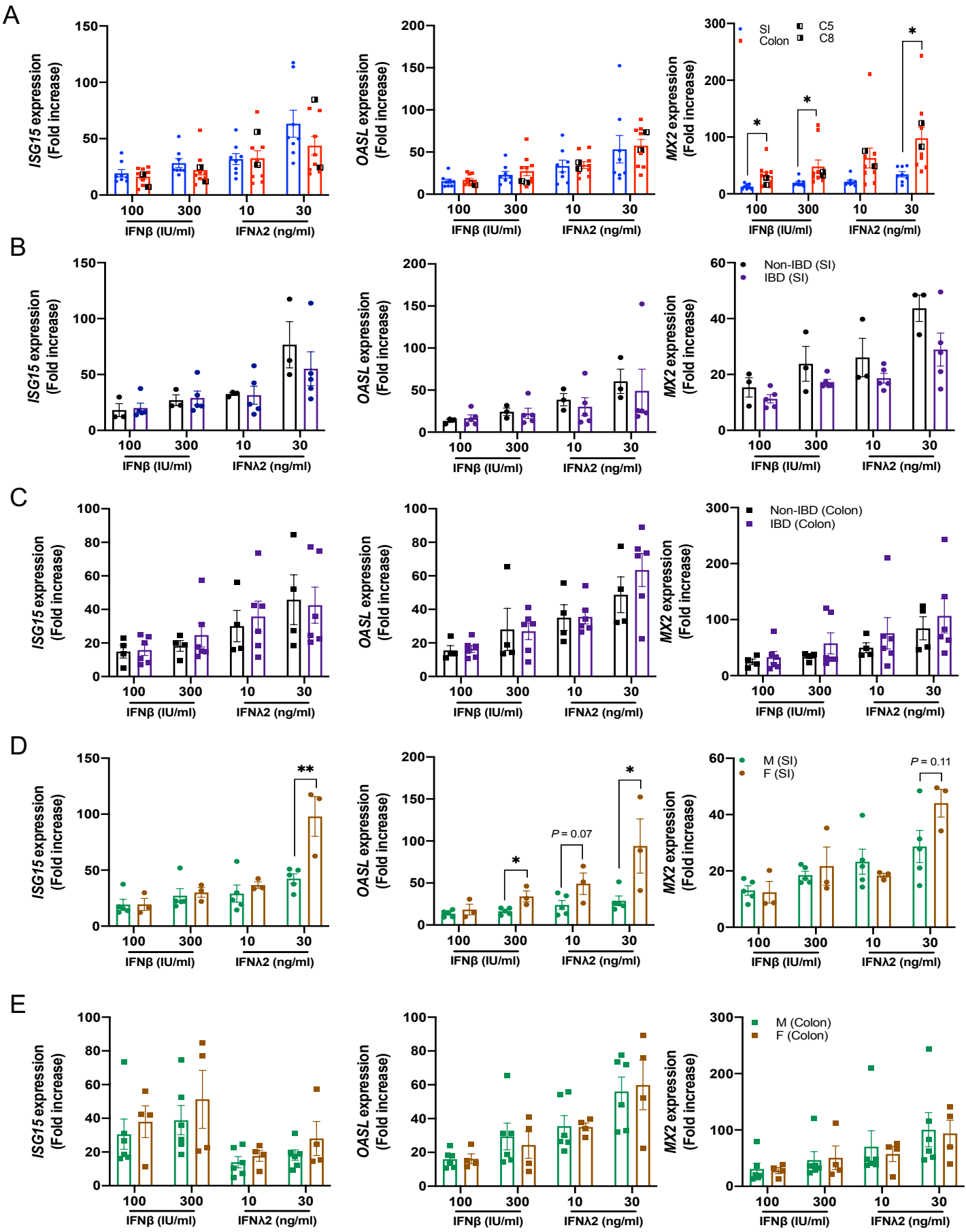
A
B
C
D
E
ISG15 expression (Fold increase)
OASL expression (Fold increase)
MX2 expression (Fold increase)
IFNβ (IU/ml)
IFNλ2 (ng/ml)
100
300
10
30
SI
Colon
C5
C8
Non-IBD (SI)
IBD (SI)
Non-IBD (Colon)
IBD (Colon)
M (SI)
F (SI)
M (Colon)
F (Colon)
P = 0.07
P = 0.11

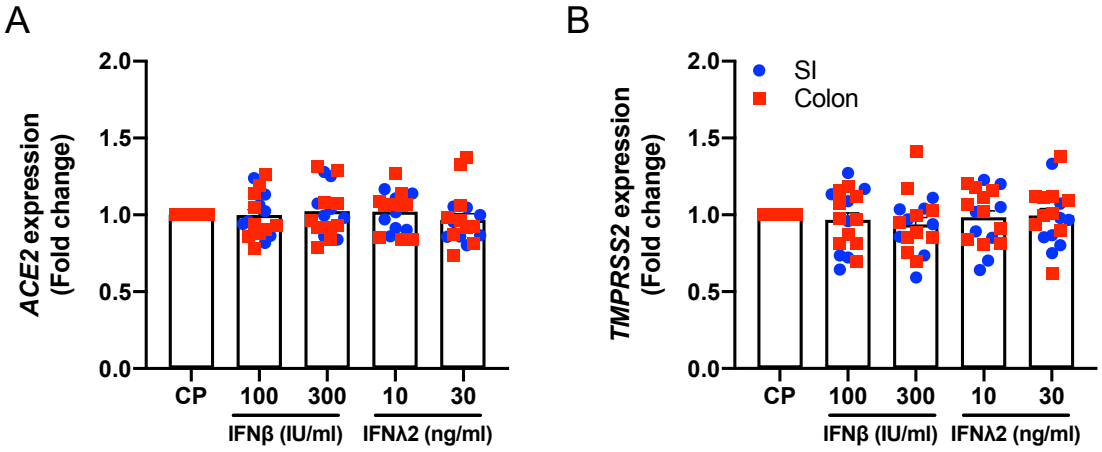
A
B
SI
Colon
ACE2 expression (Fold change)
TMPRSS2 expression (Fold change)
2.0
1.5
1.0
0.5
0.0
CP
100
300
10
30
IFNβ (IU/ml)
IFNλ2 (ng/ml)

A

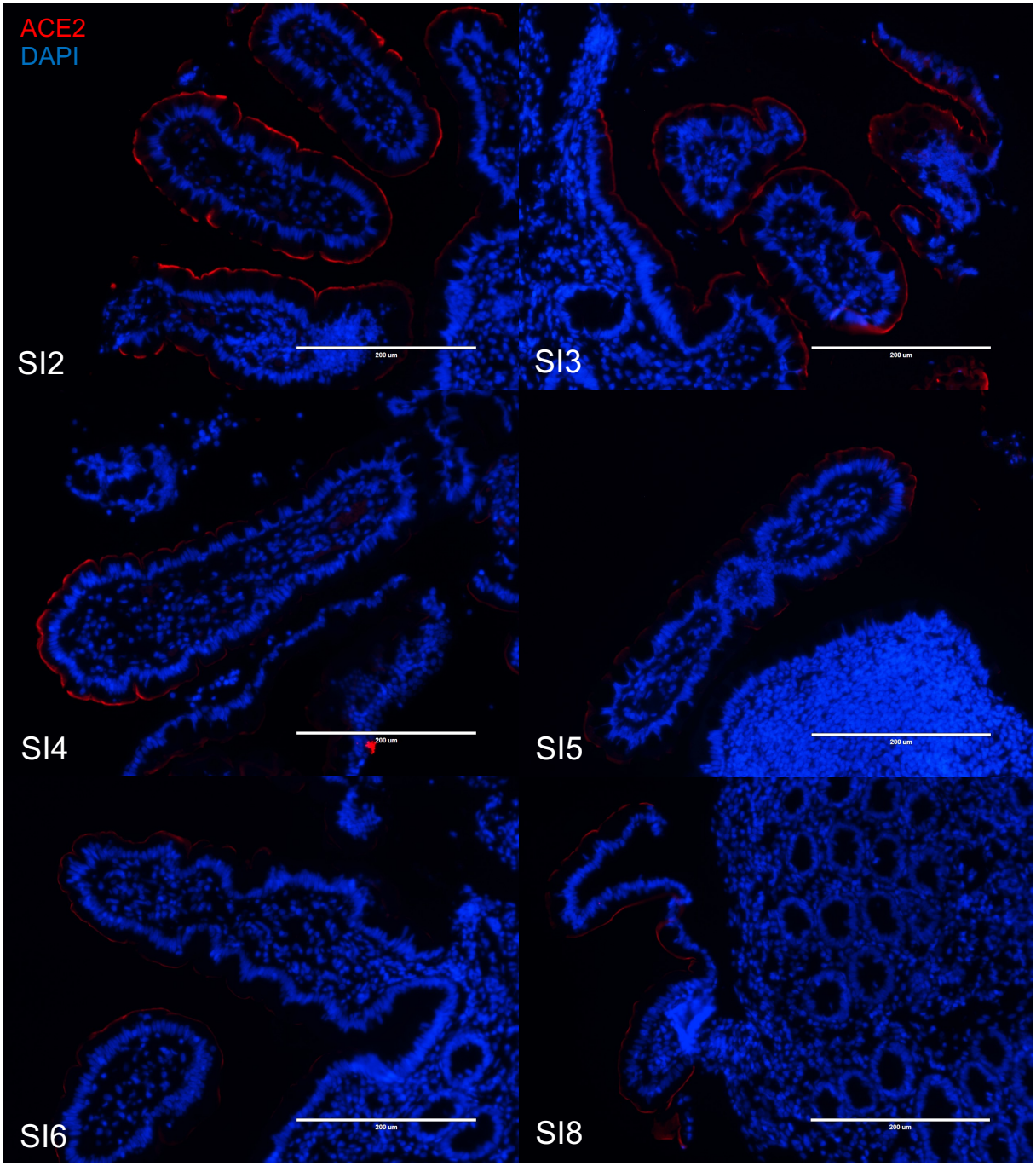
ACE2
DAPI
SI2
200 um
SI3
200 um
SI4
200 um
SI5
200 um
SI6
200 um
SI8
200 um

B

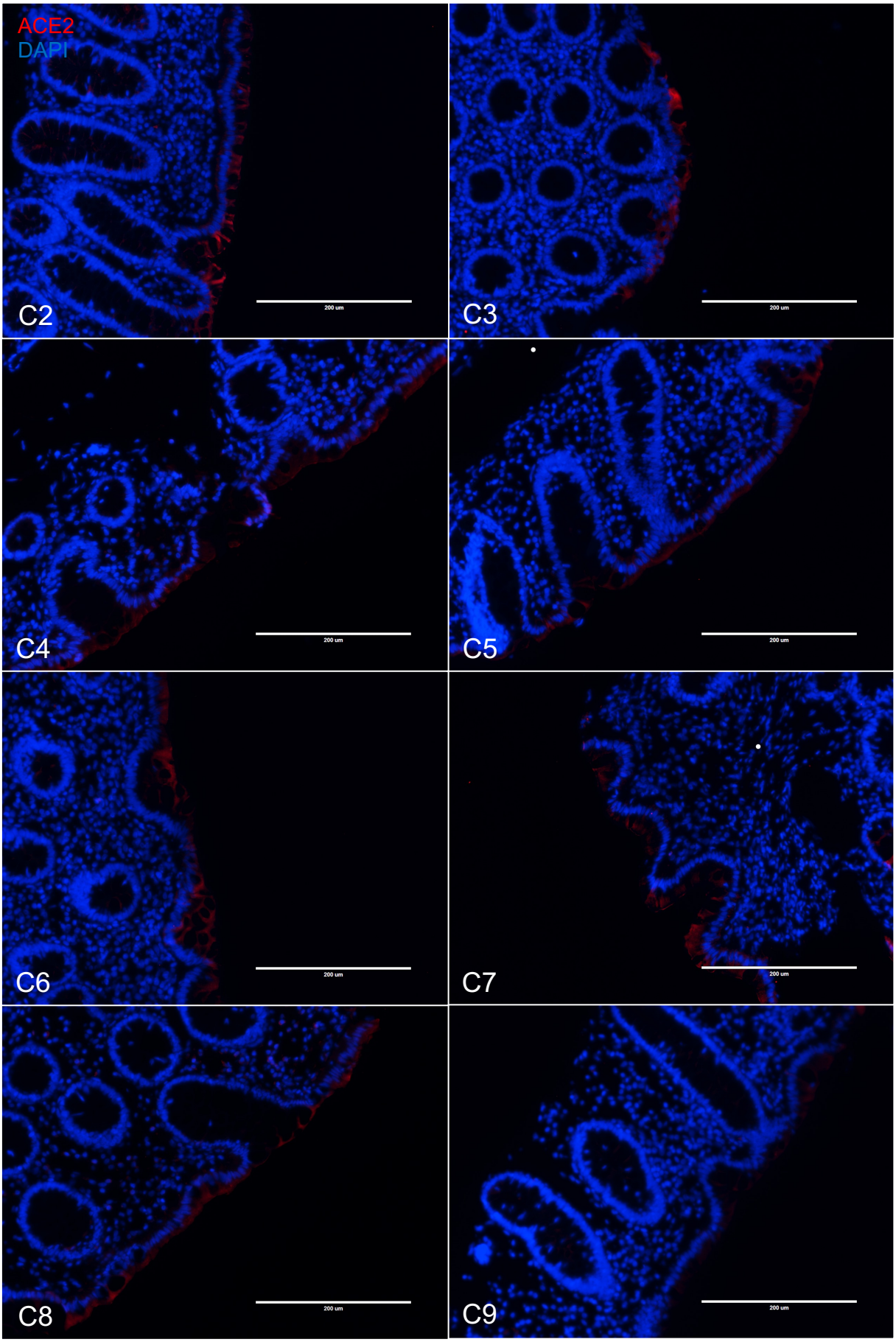
ACE2
DAPI
C2
200 um
C3
200 um
C4
200 um
C5
200 um
C6
200 um
C7
200 um
C8
200 um
C9
200 um

A

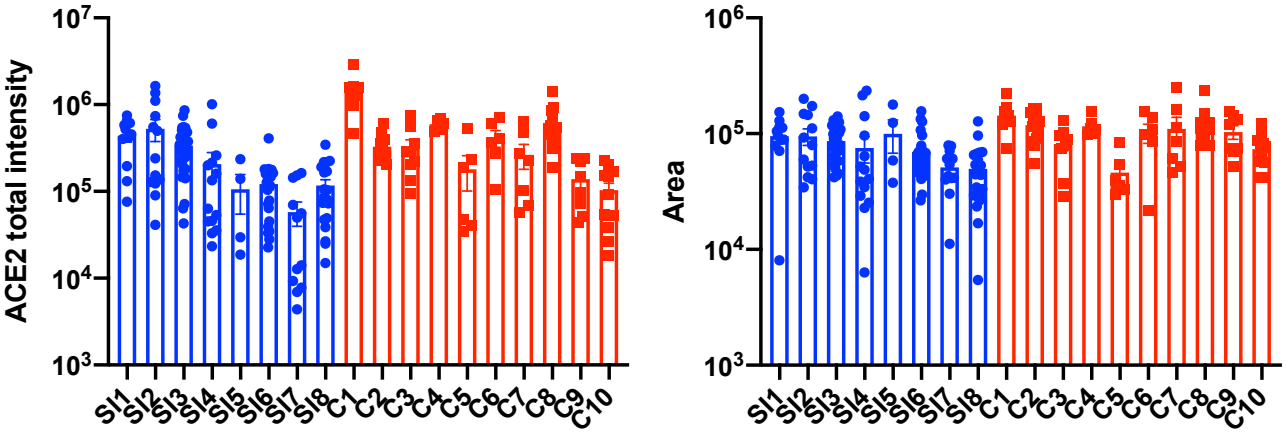
ACE2 total intensity
10^7
10^6
10^5
10^4
10^3
SI1 SI2 SI3 SI4 SI5 SI6 SI7 SI8 C1 C2 C3 C4 C5 C6 C7 C8 C9 C10
Area
10^6
10^5
10^4
10^3
SI1 SI2 SI3 SI4 SI5 SI6 SI7 SI8 C1 C2 C3 C4 C5 C6 C7 C8 C9 C10

A

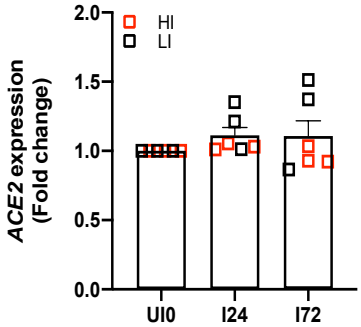

B

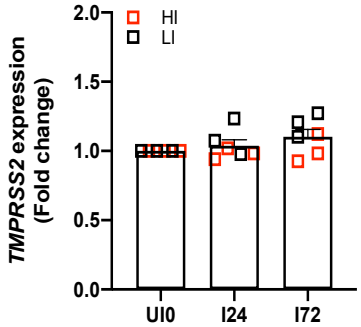

C

A vs B	Upregulated in	
	A	B
HI_UI0 vs LI_UI0	8	3
HI_UI72 vs LI_UI72	0	1
HI_I24 vs LI_I24	11	13
HI_I72 vs LI_I72	44	38
HI_UI0 vs HI_I24	10	3
HI_I24 vs HI_I72	12	180
HI_UI0 vs HI_UI72	0	0
HI_UI72 vs HI_I72	2	129
LI_UI0 vs LI_I24	7	0
LI_I24 vs LI_I72	46	207
LI_UI0 vs LI_UI72	0	0
LI_UI0 vs LI_I72	3	68

D

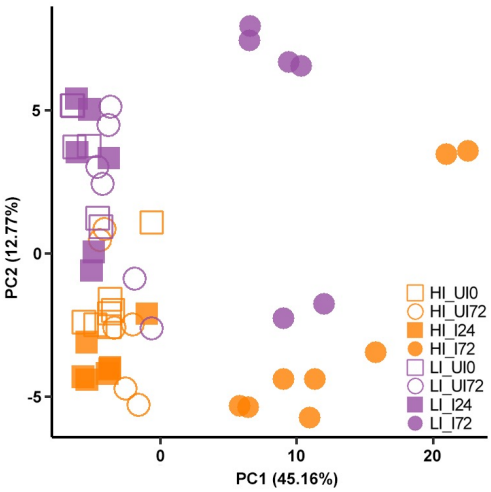

E

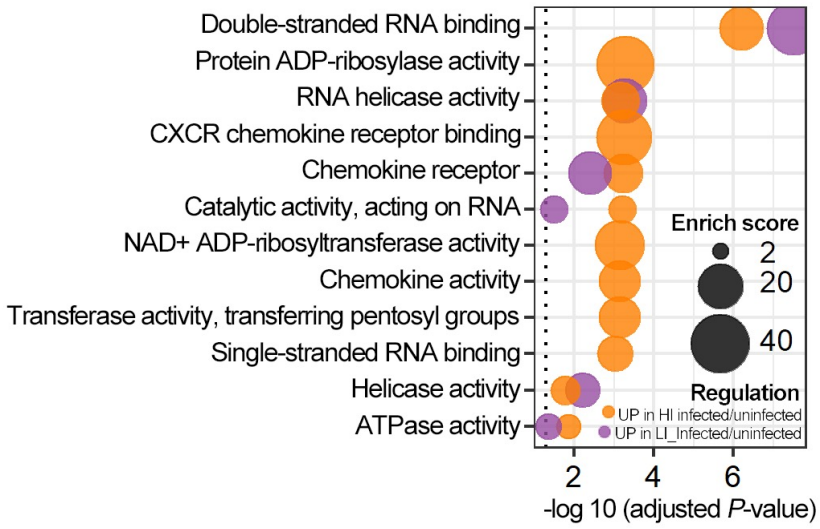

F

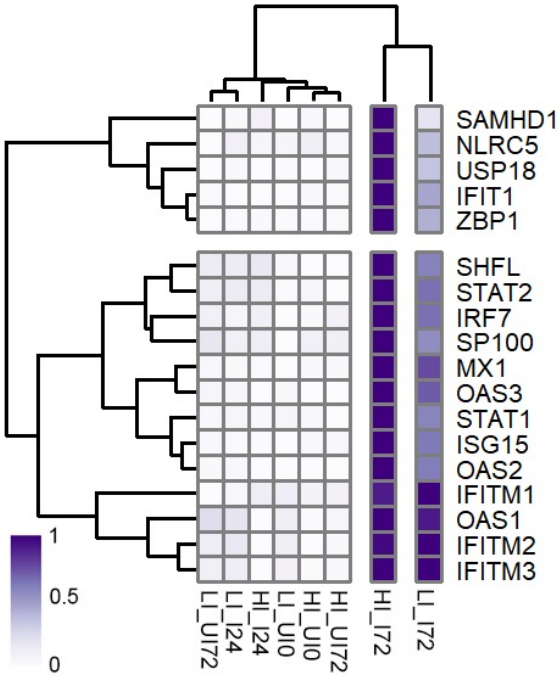

G

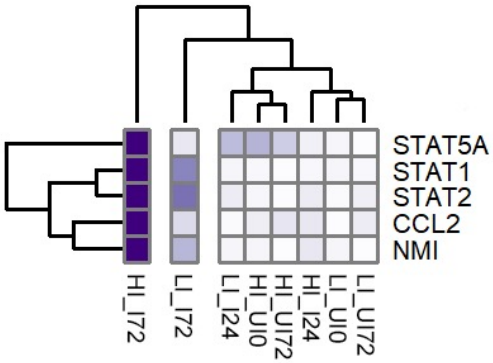
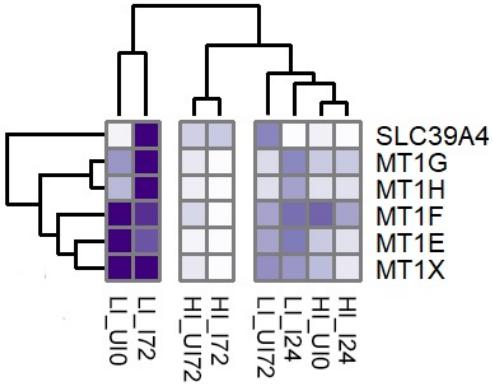
H